Subduction, underplating, and return flow recorded in the Cycladic Blueschist Unit exposed on Syros, Greece

Alissa J. Kotowski[1*], Whitney M. Behr[1,2], Miguel Cisneros[1,2], Daniel F. Stockli[1], Konstantinos Soukis[3], Jaime D. Barnes[1], Daniel Ortega-Arroyo[1†]

[1]Department of Geological Sciences, Jackson School of Geosciences, University of Texas at Austin, USA
[2]Geological Institute, Department of Earth Sciences, Swiss Federal Institute of Technology (ETH)
[3]Geology and Geoenvironment, National and Kapodistrian University of Athens, Greece

Key Points:

- Syros is a tectonic stack composed of 3 slices constructed by subduction and underplating; peak subduction ages young with structural depth.
- The subduction-to-exhumation transition is marked by kinematic rotation and cooling during decompression.
- Metamorphic geochronology indicates syn-subduction exhumation occurred continuously in an Eocene-Oligocene subduction channel.

*now at Department of Earth and Planetary Sciences, McGill University
†now at Department of Earth, Atmospheric & Planetary Sciences, Massachusetts Institute of Technology

Corresponding author: Alissa J. Kotowski, `alissa.kotowski@mcgill.ca`

Abstract

Exhumed high-pressure/low-temperature (HP/LT) metamorphic rocks provide insights into deep (∼20-70 km) subduction interface dynamics. On Syros Island (Cyclades, Greece), the Cycladic Blueschist Unit (CBU) preserves blueschist-to-eclogite facies oceanic- and continental-affinity rocks that record the structural and thermal evolution associated with Eocene subduction. Despite decades of research on Syros, the pressure-temperature-deformation history (P-T-D), and timing of subduction and exhumation, are matters of ongoing discussion. Here we show that the CBU on Syros comprises three coherent tectonic slices, and each one underwent subduction, underplating, and syn-subduction return flow along similar P-T trajectories, but at progressively younger times. Subduction and return flow are distinguished by stretching lineations and ductile fold axis orientations: top-to-the-S (prograde-to-peak subduction), top-to-the-NE (blueschist facies exhumation), and then E-W coaxial stretching (greenschist facies exhumation). Amphibole chemical zonations record cooling during decompression, indicating return flow along the top of a cold subducting slab. New multi-mineral Rb-Sr isochrons and compiled metamorphic geochronology demonstrate that three nappes record distinct stages of peak subduction (53 Ma, ∼50 Ma (?), and 47 Ma) that young with structural depth. Retrograde blueschist and greenschist facies fabrics span ∼50-40 Ma and ∼43-20 Ma, respectively, and also young with structural depth. The datasets support a revised tectonic framework for the CBU, involving subduction of structurally distinct nappes and simultaneous return flow of previously accreted tectonic slices in the subduction channel shear zone. Distributed, ductile, dominantly coaxial return flow in an Eocene-Oligocene subduction channel proceeded at rates of ∼1.5-5 mm/yr, and accommodated ∼80% of the total exhumation of this HP/LT complex.

1 Introduction

The mechanical and thermal properties of the subduction interface strongly influence the internal structure, kinematics, and dynamics of a subduction zone (e.g. Cloos, 1982; Gerya & Stöckhert, 2002; Agard et al., 2018). Along the shallow interface ($\leq$ 20 km), direct observations of the megathrust and accretionary wedge are possible through high-resolution seismic reflection imaging, ocean bottom seismometers, and ocean drilling projects (e.g. Park et al., 2002; Fagereng et al., 2019; Kimura et al., 2010). However, seismic tomography and earthquake seismology have limited spatial and temporal resolution (e.g. Rondenay et al., 2008; Calvert et al., 2011) so the geometry and internal structure of the deep interface (∼20-70+ km) remain poorly understood (Platt, 1993; Chemenda et al., 1995; Gerya & Stöckhert, 2002; Agard et al., 2018).

The deep interface can be studied through geologic observations of exhumed high-pressure/low-temperature (HP/LT) metamorphic rocks. Some of the most spectacular examples – for example, the Franciscan Complex (e.g. Cloos, 1986; Wakabayashi, 1990), and the Mediterranean region (e.g. Platt et al., 1998; Jolivet et al., 2003; Brun & Faccenna, 2008) – have profoundly shaped our understanding of subduction and exhumation processes. Specifically, field studies provide constraints on the structural and kinematic evolution, interface geometry, metamorphic pressure-temperature (P-T) trajectories, and timing and rates of subduction and exhumation (e.g. Behr & Platt, 2012; Ukar et al., 2012; Dragovic et al., 2015; Angiboust et al., 2016; Agard et al., 2018; Xia & Platt, 2017; Platt et al., 2018). Geologic observations can validate or challenge the results of geodynamic simulations that model the kinematics and dynamics of rock within plate boundary shear zones (e.g. Cloos, 1982; Gerya & Stöckhert, 2002; Gerya et al., 2002; Warren et al., 2008).

Syros Island, located in the central Aegean Sea (Fig. 1), is an ideal locality to study deep interface processes due to its exceptional preservation and exposure of HP/LT blueschist-to-eclogite facies assemblages (Dürr et al., 1978; Ridley, 1982, 1984; Okrusch & Bröcker, 1990). Despite decades of research on Syros, there are many disagreements regarding the structural evolution, metamorphic conditions, and timing and mechanisms of

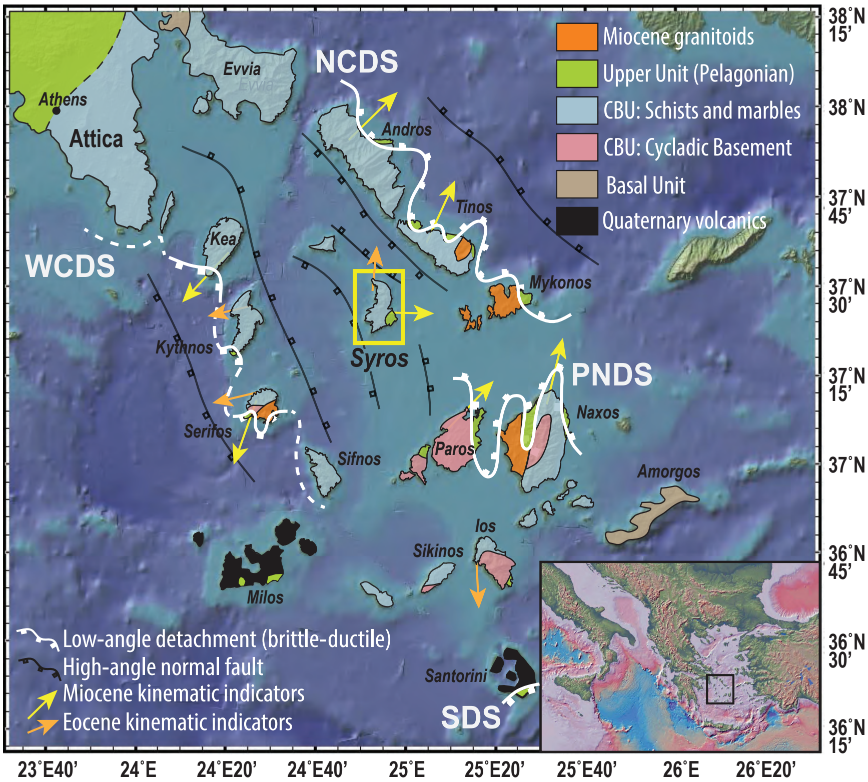

Figure 1: Regional tectonic map of the Cyclades, modified from Grasemann et al. (2012). Syros is outlined by the yellow box. North Cycladic (NCDS), West Cycladic (WCDS), Paros-Naxos (PNDS), and Santorini (SDS) Detachment Systems are outlined in white.

subduction and exhumation on the island (e.g. Ridley, 1982; Trotet et al., 2001a; Rosenbaum et al., 2002; Ring & Layer, 2003; Keiter et al., 2004; Schumacher et al., 2008; Soukis & Stockli, 2013; Bröcker et al., 2013; Laurent et al., 2016; Lister & Forster, 2016; Aravadinou & Xypolias, 2017; Laurent et al., 2018; Skelton et al., 2019). Furthermore, crustal-scale extensional detachments that accommodated the latest stages of post-orogenic exhumation are well-documented across the Cyclades (Avigad & Garfunkel, 1989, 1991; Gautier et al., 1993; Jolivet et al., 2010; Jolivet & Brun, 2010; Grasemann et al., 2012; Soukis & Stockli, 2013; Schneider et al., 2018), but workers still debate the relative importance of major detachments during syn-orogenic exhumation from peak conditions, and whether strain was distributed or highly localized (Rosenbaum et al., 2002; Keiter et al., 2004; Bond et al., 2007; Lister & Forster, 2016; Laurent et al., 2016).

In this work, we present new structural and petrologic data and Rb-Sr geochronology, and integrate our results with synthesized geochronology, to present a new model for the evolution of the CBU on Syros. Our results refine the island's deformation-metamorphism history, and shed light on the kinematics, metamorphic conditions, and timing of subduction and return flow in the Hellenic subduction zone. This work has direct implications for rates and mechanisms of HP/LT rock exhumation, and provides a broader framework for regional construction of the Attic-Cycladic Complex.

2 Regional Geologic Setting

The Cycladic Islands and parts of mainland Greece are part of the Attic-Cycladic Complex (ACC), which is divided into three units according to depositional age and metamorphic history. From structural top to bottom, the units are: (1) the Upper Cycladic Nappe; (2) the Cycladic Blueschist Unit; and (3) the Basal Unit (e.g. Dürr et al., 1978; van der Maar & Jansen, 1983; Jacobshagen, 1986; Avigad & Garfunkel, 1989; Altherr et al., 1994) (Fig. 1). The Upper Cycladic Nappe is a suite of ophiolitic slivers, altered carbonates ± serpentinites, Late Cretaceous (70-100 Ma) amphibolite-facies orthogneisses, and Miocene greenschist-facies meta-basalts, and correlates with the Pelagonian Unit exposed on mainland Greece (Papanikolaou, 1987). The Upper Nappe was the upper plate during Late Cretaceous-Paleogene subduction and crops out above the Cycladic Blueschist Unit (CBU) in the hanging wall of crustal-scale, Miocene detachment faults on several Cycladic Islands (Jolivet et al., 2010, 2013; Soukis & Stockli, 2013).

The majority of the ACC is composed of the Cycladic Blueschist Unit (CBU) (Fig. 1). The CBU comprises poly-metamorphosed tectonic slices (Dürr et al., 1978; Forster & Lister, 2005, 2008; Jolivet & Brun, 2010) of the following protoliths: (1) (Jurassic?-to-) Cretaceous (∼80 Ma) mafic igneous crust with enriched-MORB and back-arc geochemical signatures ± serpentinized mantle (Bonneau, 1984; Seck et al., 1996; Tomaschek et al., 2003; Bulle et al., 2010; Fu et al., 2015; Cooperdock et al., 2018), (2) Triassic (∼240 Ma) bimodal rift volcanics (Keay, 1998; Robertson, 2007; Löwen et al., 2015) blanketed by Triassic-to-Cretaceous, locally-sourced, rifted and passive continental margin siliciclastic and carbonate rocks (Papanikolaou, 2013; Löwen et al., 2015; Seman, 2016; Seman et al., 2017; Poulaki et al., 2019), and (3) peri-Gondwanan basement cross-cut by Carboniferous calc-alkaline granitoids (Keay, 1998; Keay & Lister, 2002; Flansburg et al., 2019).

CBU lithologies record evidence for Eocene (∼53-45 Ma) HP/LT metamorphism under blueschist-to-eclogite facies conditions ('M1') (Dixon, 1976; Schliestedt, 1986; Okrusch & Bröcker, 1990; Wijbrans et al., 1990; Tomaschek et al., 2003; Lagos et al., 2007; Laurent et al., 2017) and were exhumed first within the subduction channel and then in the footwalls of crustal-scale normal faults of the North and West Cycladic (e.g. Jolivet et al., 2003; Ring et al., 2003; Jolivet & Brun, 2010; Jolivet et al., 2010; Grasemann et al., 2012; Soukis & Stockli, 2013; Ring et al., 2020), the Paros-Naxos (Gautier et al., 1993), and the Santorini Detachment Systems (Schneider et al., 2018). Exhumation beneath ductile and semi-brittle detachments locally produced a greenschist-facies ('M2') overprint (Bröcker, 1990; Bröcker et al., 1993). As slab rollback ensued and the arc migrated southward through the former forearc, Miocene I-type plutons intruded the exhuming CBU and led to a local high-temperature, amphibolite-facies ('M3') overprint on some islands (e.g. Paros and Naxos) (Andriessen et al., 1979; Pe-Piper et al., 2002; Brichau et al., 2007).

3 The CBU on Syros Island

3.1 Rock types and tectonostratigraphy

Syros is a small island (∼84 km^2) in the central Cyclades and is dominantly composed of CBU with a klippe of UU in the southeast in the hanging wall of the Oligo-Miocene Vari Detachment (Ridley, 1984; Ring et al., 2003; Keiter et al., 2011; Soukis & Stockli, 2013) (Fig. 1). In the context of the Cyclades, Syros best preserves the regional HP/LT metamorphic event (Ridley, 1982; Okrusch & Bröcker, 1990).

Within the CBU on Syros, mafic blueschists and eclogites crop out along three tectonostratigraphic horizons: Kampos Belt, Kini-Vaporia-Kalamisia, and Galissas-Fabrikas. Each horizon exposes ∼300-500 m (structural thickness) of blueschist-to-eclogite facies meta-basalts and gabbros, serpentinites, and bimodal blueschist-quartz schist meta-volcanics in varying proportions. Along Kampos Belt, eclogitic meta-gabbros, blueschist facies bimodal meta-volcanics, and serpentinite/chlorite-talc schists are most abundant (Ridley,

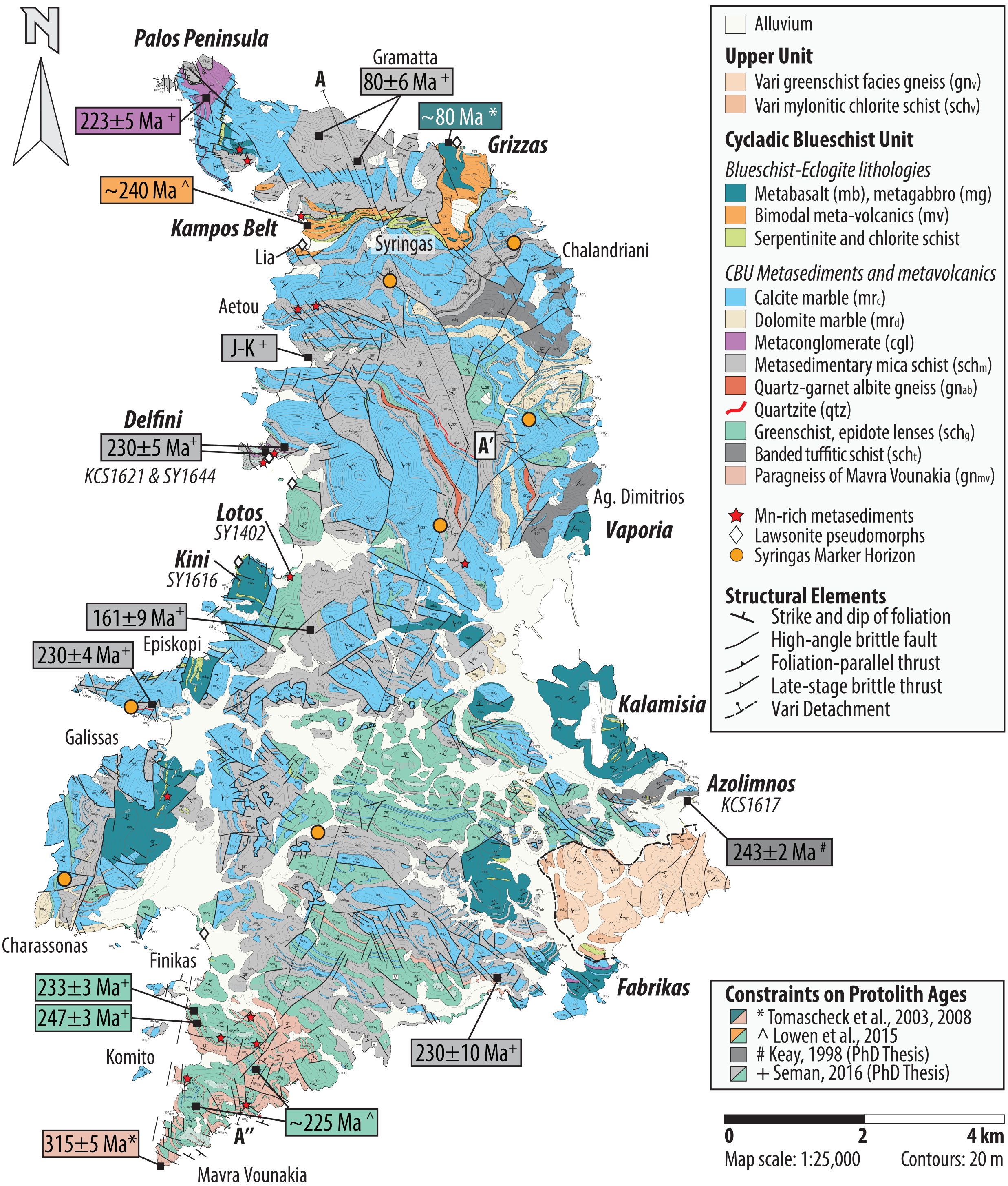

Figure 2: Geologic and structural map of Syros Island, modified from Keiter et al. (2004, 2011). Structural elements and locations of the Syringas Marker Horizon are from Keiter et al. (2011). Constraints on protolith ages are from the references discussed in Section 3.1. Protolith ages are color coded according to rock type. Localities discussed in this study are shown in bold italics, new Rb-Sr sample names and locations are in italics.

1982; Dixon & Ridley, 1987; Keiter et al., 2011) (Fig. 2). Kini, Vaporia (north of Ermoupoli), and Kalamisia are primarily composed of fine-grained mafic blueschist, and contain pods and lenses of eclogite (centimeters-to-decimeters in diameter) and meters-thick layers of serpentinite/talc schist (Keiter et al., 2011; Kotowski & Behr, 2019). Fabrikas comprises coarse-grained glaucophane-bearing eclogites (centimeters to meters in diameter) within a fine-grained matrix of mafic blueschists and quartz-mica schists, capped by meta-carbonate (Skelton et al., 2019; Kotowski & Behr, 2019; Ring et al., 2020). Keiter et al. (2011) suggested that mafic blueschists and eclogites are genetically related, and changes in volume proportions of lithologies reflect primary lateral and/or vertical 'facies changes' of an enriched-MORB or back-arc igneous suite.

The majority of the CBU comprises a ~6-8 km section of intercalated meta-volcanic and meta-sedimentary schists, and calcite- and dolomite-marbles with Jurassic-to-Cretaceous depositional ages (Keiter et al., 2004; Papanikolaou, 2013; Löwen et al., 2015; Seman et al., 2017) (Fig. 2). Keiter et al. (2004, 2011) documented a series of boudinaged marbles, cherts, and albite-bearing quartzite, which they named the Syringas Marker Horizon (orange dots on Fig. 2). The sequence crops out at 3 or 4 structural levels and appears to never be overturned, suggesting it marks several km-scale thrust sheets as opposed to megafolds, and may reflect relict primary sedimentary layering (Ridley, 1982; Dixon & Ridley, 1987; Keiter et al., 2011). Keiter et al. (2011) also documented repetition of distinct packages of bimodal, rift-related meta-volcanics (also mapped as "banded tuffitic schists") that have Triassic magmatic protolith ages (Keay, 1998; Pe-Piper et al., 2002; Löwen et al., 2015; Seman, 2016) (Fig. 2), which appears to be further evidence for imbrication.

Detrital zircon (DZ) U-Pb geochronology and Maximum Depositional Ages (MDAs) of meta-sediments support that 'cryptic thrusts' exist. With dense sampling throughout the structural pile, Seman (2016) documented: (1) A conformable relationship between Kampos Belt meta-igneous rocks and the overlying Gramatta meta-sedimentary package; and (2) three horizons in the underlying CBU where old-on-young MDA inversions occur. For example, Triassic meta-volcanics of Kampos Belt are thrust on top of Cretaceous meta-sediments south of Aetou, and Triassic meta-volcanics at Delfini are thrust atop Cretaceous meta-sediments east of Kini (Fig. 2). Seman (2016) concluded that Syros comprises 3 or 4, ~3 km thick slivers of imbricated meta-sedimentary rocks.

3.2 Previously proposed P-T-D-t paths

Previously published P-T-D evolutions for Syros fall into two categories. Some workers have argued that the majority of deformation and metamorphism on the island is exhumation-related (Trotet et al., 2001a; Laurent et al., 2016; Lister & Forster, 2016) (Fig. 3A). These studies interpret mafic blueschists and eclogites to occupy the top of the structural pile and separate them from underlying meta-sedimentary rocks along extensional shear zones (Trotet et al., 2001b; Forster & Lister, 2005; Laurent et al., 2016, 2018). An implication of this model is that distinct rock types were juxtaposed late in their histories during syn-orogenic exhumation (Forster & Lister, 2005; Laurent et al., 2016). Therefore, lithologic packages that currently occupy different structural depths could have followed different P-T paths (cf. Trotet et al., 2001b, 2001a; Laurent et al., 2018), and/or could have been subducted at different times (Lister & Forster, 2016; Laurent et al., 2017). This model could potentially explain reported differences in P-T estimates across Syros; mafic blueschists and eclogites may have been subducted deeper, earlier, compared to meta-sedimentary lithologies (as discussed by Schumacher et al. (2008)).

Alternatively, other work has suggested that prograde deformation and metamorphism on the island are locally preserved, and exhumation-related strain was partitioned into weaker lithologies (Ridley, 1982; Rosenbaum et al., 2002; Keiter et al., 2004; Bond et al., 2007; Keiter et al., 2011) (Fig. 3A). These studies interpret mafic blueschist and eclogites to record primary relationships with surrounding schists and marbles, or to have been jux-

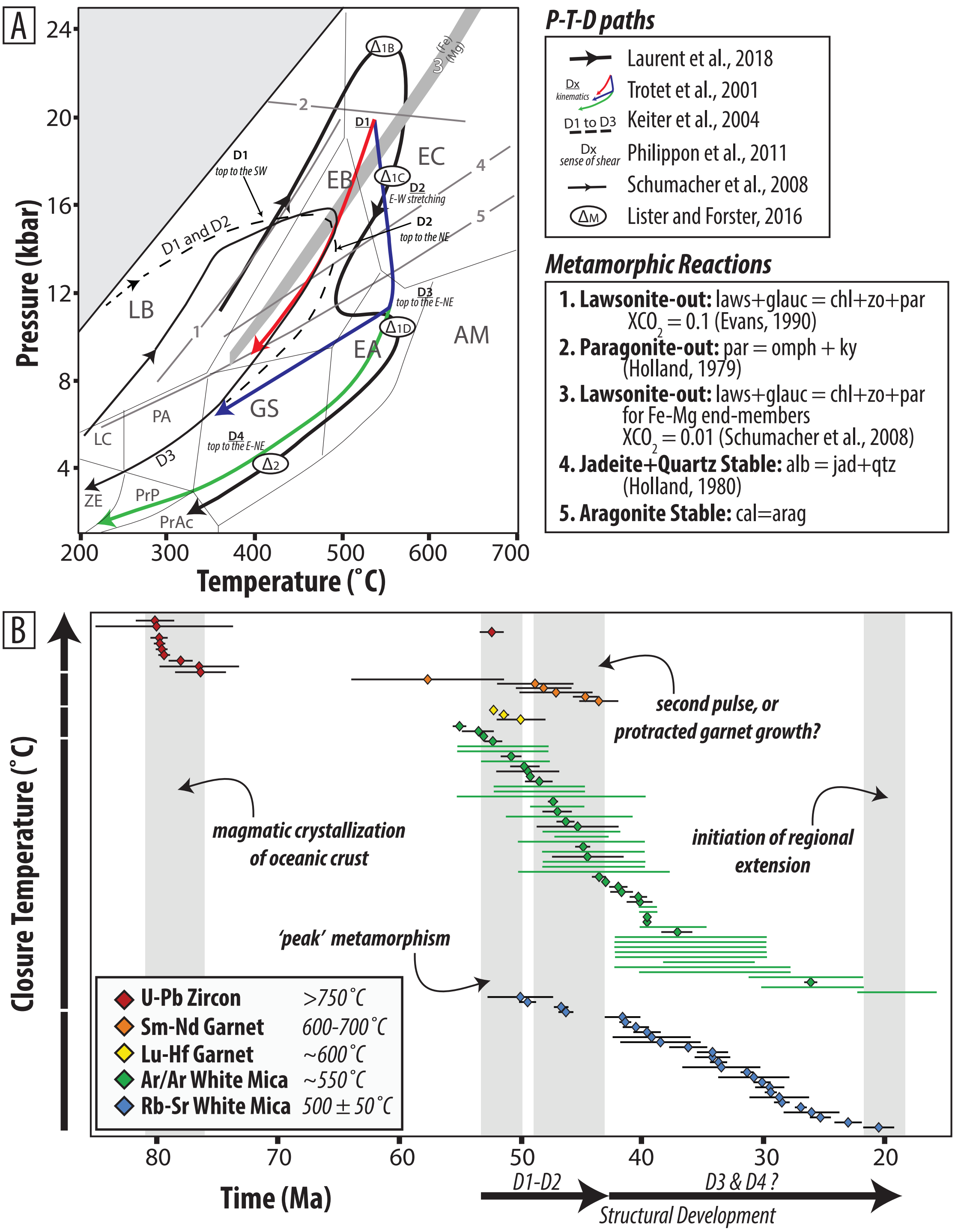

Figure 3: (A) Compilation of proposed P-T-D histories for the CBU on Syros. (B) Closure temperature vs. time for compiled metamorphic geochronology listed in Table A2. This dataset comprises 100 datapoints made up of 185 individual ages (some data clusters are weighted means), from 16 studies and 5 chronometers, from work published during the interval 1987-2019.

taposed with the schists and marbles during early thrusting (Blake Jr et al., 1981; Ridley, 1982; Hecht, 1985; Keiter et al., 2004). Either way, mafic blueschists and eclogites need not be separated from surrounding CBU by faults or shear zones, but instead could occupy a range of structural depths throughout the structural pile (Keiter et al., 2004). This model implies that meta-mafic and meta-sedimentary rocks that occupy similar structural levels were subducted together and experienced similar P-T histories through subduction and exhumation (Schumacher et al., 2008; Keiter et al., 2011).

Existing metamorphic ages do not help distinguish prograde from retrograde fabrics, nor the timing of subduction vs. exhumation, so differentiating between these P-T-D evolutions has been challenging (Fig. 3B). Two age clusters are commonly cited for the timing of peak subduction on Syros: ∼53-50 Ma (U-Pb zircon, Ar/Ar and Rb-Sr white mica, Lu-Hf garnet; Tomaschek et al. (2003); Lagos et al. (2007); Lister and Forster (2016); Cliff et al. (2016)), and both ∼52 Ma *and* ∼45 Ma for different underplated slices (Ar/Ar white mica; Forster and Lister (2005); Lister and Forster (2016); Laurent et al. (2017)). Garnet Sm-Nd and Lu-Hf ages span the proposed range, thus raising the question of whether garnet growth reflects two pulses or continuous growth at peak conditions (cf. Kendall, 2016). Furthermore, Ar/Ar and Rb-Sr ages span the entire Eocene. Maximum temperatures do not appear to have exceeded those required for diffusional resetting of the Ar/Ar and Rb-Sr systems, but it is unclear whether retrograde blueschist-to-greenschist facies white mica ages record incomplete isotopic mixing or continuous recrystallization (Fig. 3B) (e.g. Bröcker et al., 2013; Rogowitz et al., 2015; Cliff et al., 2016; Laurent et al., 2017; Uunk et al., 2018). An additional challenge is that many geochronologic data points in Figure 3B were collected without a clear framework for linking the ages to specific fabric-forming events.

Much effort has been made to synthesize structure, petrology, and geochronology across Syros (e.g. Keiter et al., 2011; Laurent et al., 2018) and the Cyclades (e.g. Forster & Lister, 2005, 2008; Philippon et al., 2012; Laurent et al., 2017). However, several key components of the subduction history remain unclear, including the structural relationships between mafic blueschist and eclogites and surrounding schists and marbles, the P-T-D evolution recorded in the CBU nappes, and the timing of subduction and exhumation as a function of structural depth. Herein, we address these issues by combining structural observations, petrology, and new petrochronology supplemented by synthesized age constraints.

4 Structures and Deformation Fabrics

The CBU on Syros records evidence for three main phases of deformation and metamorphism, herein referred to as D_R, D_S, and D_{T1-2} (Table 1). Each phase led to spaced to penetrative foliation development, and/or ductile folding of older foliations. Kinematic indicators, metamorphic mineral assemblages, and porphyroblast zonations demonstrate that D_R and D_S developed on the prograde path and are best preserved in mafic blueschists and eclogites (but are locally preserved as textural relicts in bimodal meta-volcanics and meta-sediments), and D_T developed on the retrograde path and is best recorded by meta-volcanic and meta-sedimentary schists.

4.1 D_R – Prograde fabric development during subduction under blueschist-facies conditions

D_R is the earliest recognizable prograde event but it is not visible at the outcrop-scale. D_R likely formed a strong, penetrative S_R foliation that is locally recorded as inclusion trails in garnet porphyroblasts at Kampos (Fig. 6A,B) and is tightly folded during D_S. Inclusion trails are orthogonal to the external foliation and are defined by glaucophane, omphacite, and white mica.

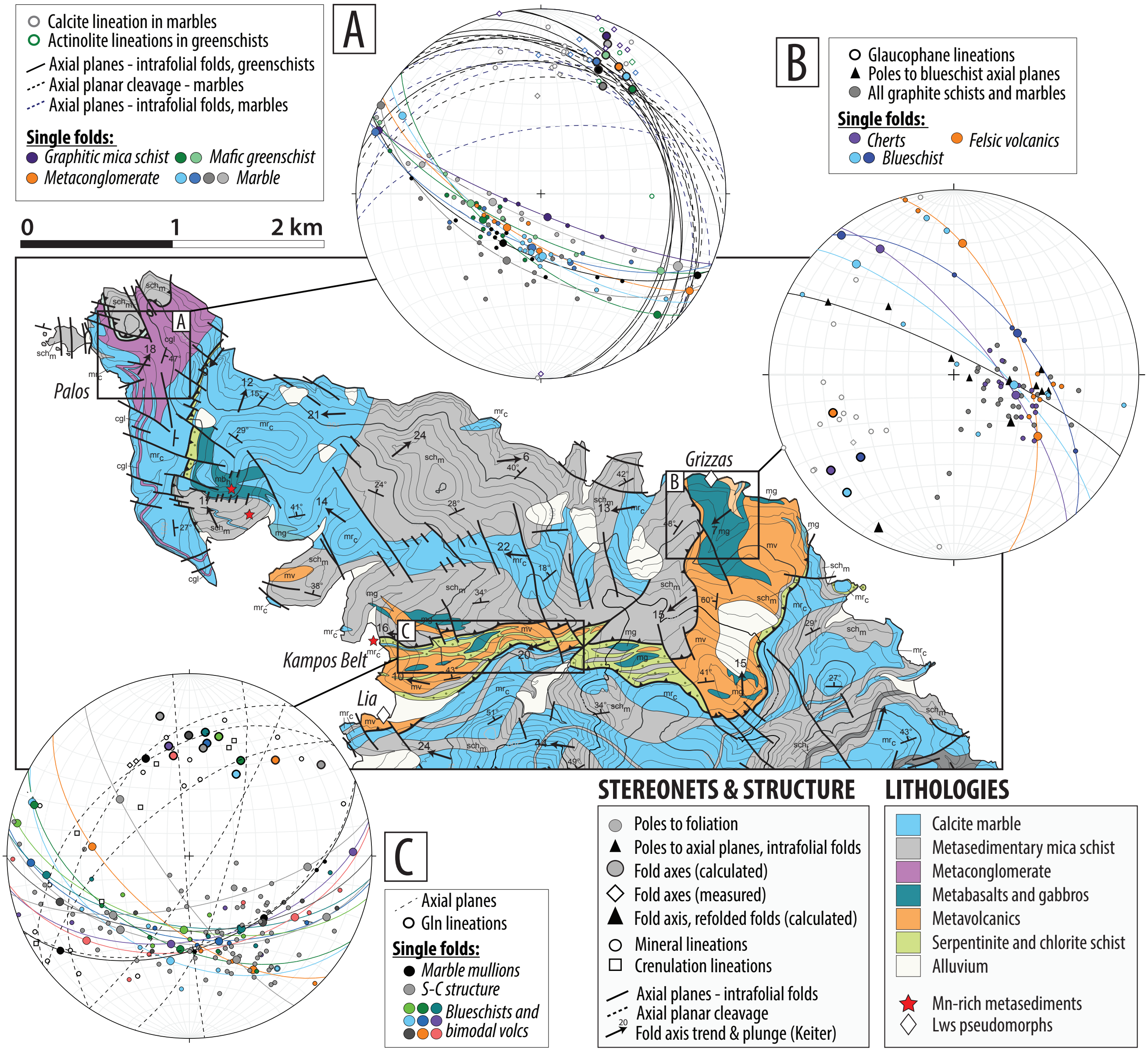

Figure 4: Geology and structural elements of Northern Syros. Base map, foliation orientations, and fold axes (black arrows) are from Keiter et al. (2011). Foliations are plotted as poles (unless otherwise specified), and colored best-fit planes are π circles. Topographic contours are 20 m. Data plotted in stereonets were collected from the areas outlined by solid black boxes. See text for description of structural elements.

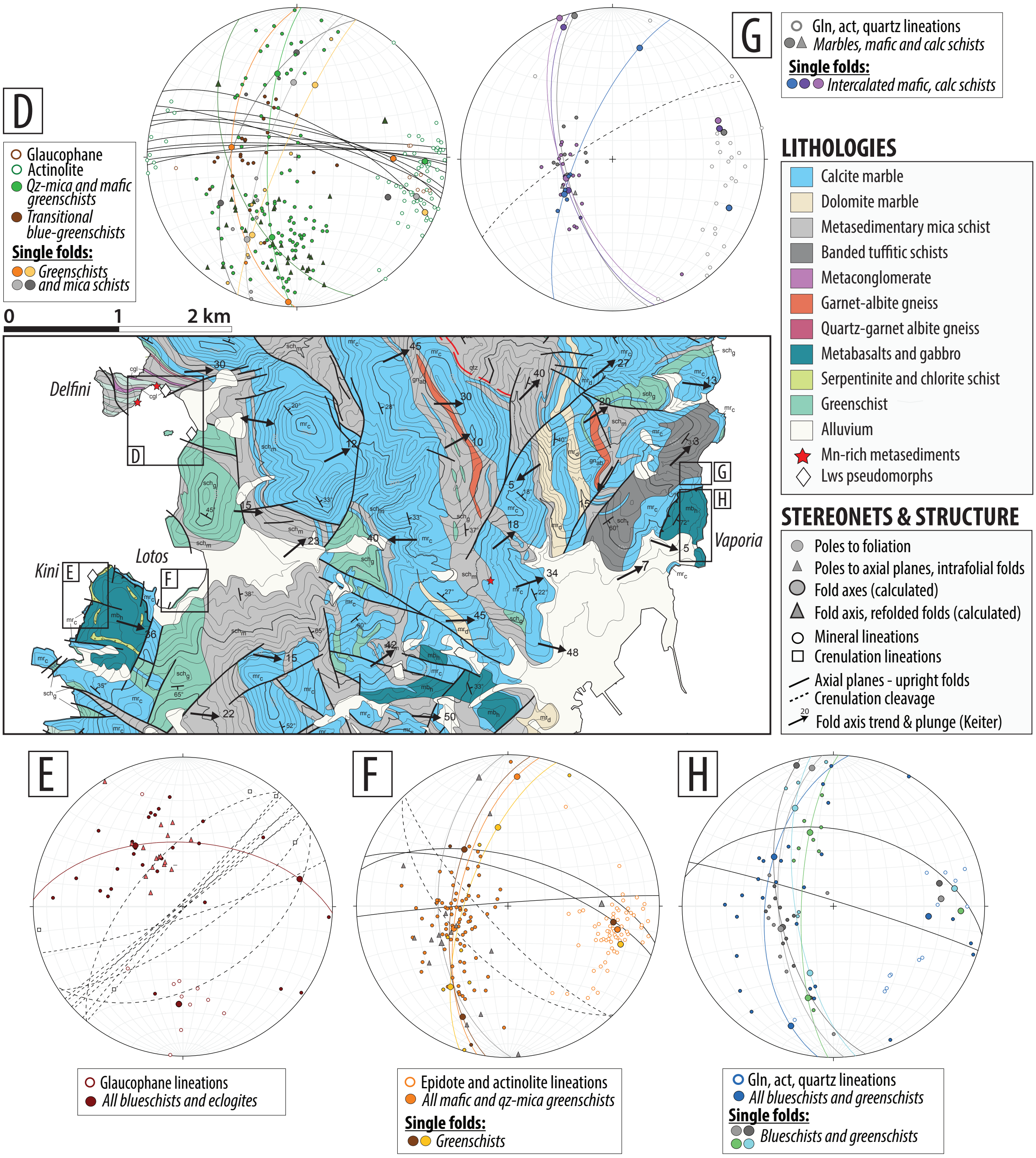

Figure 4: Continued. Geology and structural elements of Central Syros.

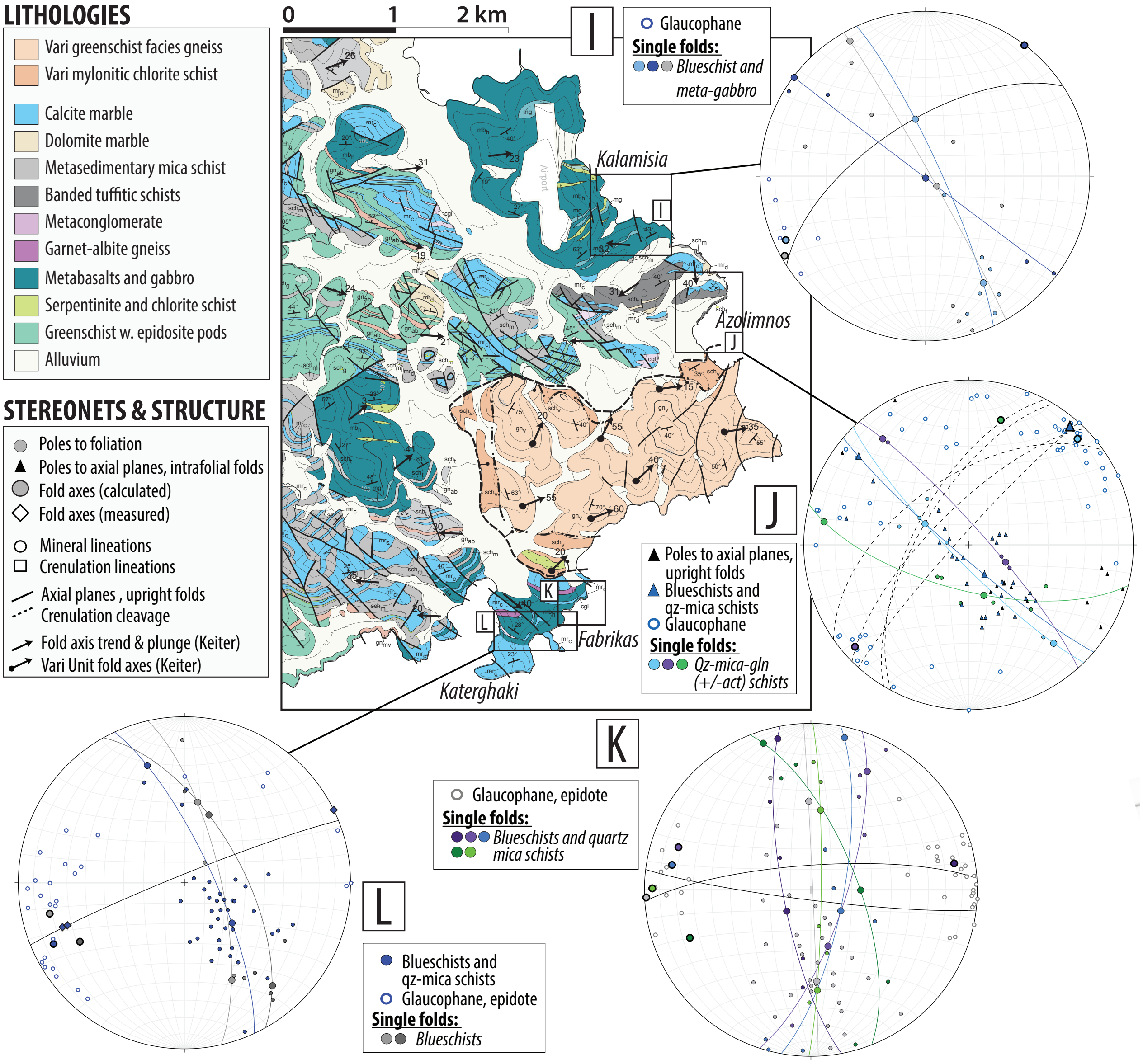

Figure 4: Continued. Geology and structural elements of Southeast Syros. Black arrows with the circles are fold axes in the Vari Unit.

Event	Context	Diagnostic Structures		Metamorphism	Best Exposure
D_R	Subduction	• Only preserved as inclusion trails in garnets and as early fabric (S_R) that is tightly folded during D_S	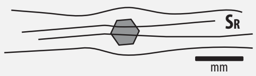	lawsonite-blueschist	N/A
D_S	Subduction to near-peak conditions	• Axial plane schistosity (S_S) associated with tight to isoclinal folds (F_S) that transpose the S_R foliation, with S-SW-plunging fold axes • S-SW mineral and stretching lineations • Dominantly non-coaxial, locally non-penetrative in mafic lenses (e.g. Grizzas)	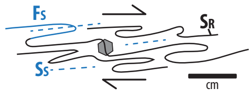	lawsonite blueschist-to-eclogite	Grizzas Kini
$D_{T1\text{-}2}$	Exhumation	• Crenulation cleavage (S_T) associated with upright, open-to-tight folds (F_T) that fold S_S • Fold axes and mineral lineations rotate from N-NE (D_{T1}) to E-W (D_{T2}) as a function of strain • Dominantly coaxial, but locally non-coaxial near the Vari Detachment (e.g. Fabrikas, Kalamisia) • Ductile to semi-brittle boudinage in later stages	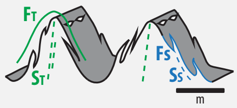	epidote-blueschist progressing to greenschist	Kampos (early) Azolimnos (early) Delfini (later) Lotos (later)

Table 1: Summary of interpreted deformation-metamorphism events in the CBU on Syros.

4.2 D_S – Prograde-to-peak fabric development during subduction under blueschist- to eclogite-facies conditions

Deformation stage D_S captures peak metamorphic conditions, and produced: (1) an axial plane schistosity, S_S, associated with tight to isoclinal folds (F_S) that have S-SW-plunging fold axes and fold S_R; (2) SSW-to-S-plunging mineral lineations; (3) a blueschist-to-eclogite facies fabric containing syn-kinematic garnet, omphacite, and (now pseudomorphed) lawsonite porphyroblasts; and (4) chemical zonations in glaucophane and omphacite that record syn-kinematic increase in pressure and temperature.

4.2.1 D_S Structures

D_S is best recorded at Grizzas and Kini (Fig. 4E), with relicts preserved on Kampos Belt (Fig. 4C), at Lia Beach, and at Azolimnos (Fig. 4J). D_S produced a dominant S_S foliation in mafic blueschists, meta-cherts, and bimodal meta-volcanics at Grizzas that is parallel to the axial planes of intrafolial folds (F_S), and transposed and boudinaged quartz veins. This folding event is characterized by shallowly to moderately plunging SW-trending fold axes clustering around 205-251°/15-35°; glaucophane mineral lineations are similarly oriented (Fig. 4B). In rare cases, outcrop-scale prograde metamorphism was not associated with penetrative deformation, indicated by preservation of igneous protolith features such as pillow lavas (Grizzas, cf. Keiter et al. (2011)) and magmatic breccias (e.g. at Grizzas, Episkopi, Fig. 5A).

Kini is bounded by high-angle normal faults and is structurally discordant with respect to the surrounding CBU (Fig. 4E; cf. Keiter et al. (2011)). In one location, serpentinite wraps around the base of massive meta-gabbros, which transitions upward into fine-grained blueschists, suggesting local preservation of an attenuated section of metamorphosed oceanic lithosphere (Fig. 5B). Similar to Grizzas, the D_S fabric in Kini blueschists contains isoclinal folds (F_S) with shallowly south-plunging fold axes. This fold generation is recorded by a 182°/33° fold axis in Kini schists (Fig. 4E; Fig. 5D). The S_S axial planar cleavage (e.g. Fig. 5E) seen in Kini mafic blueschists (e.g. Fig. 5E) is also seen as textural relicts in quartz-mica rich lithologies, as at Azolimnos (Fig. 5G). In some localities, glaucophane

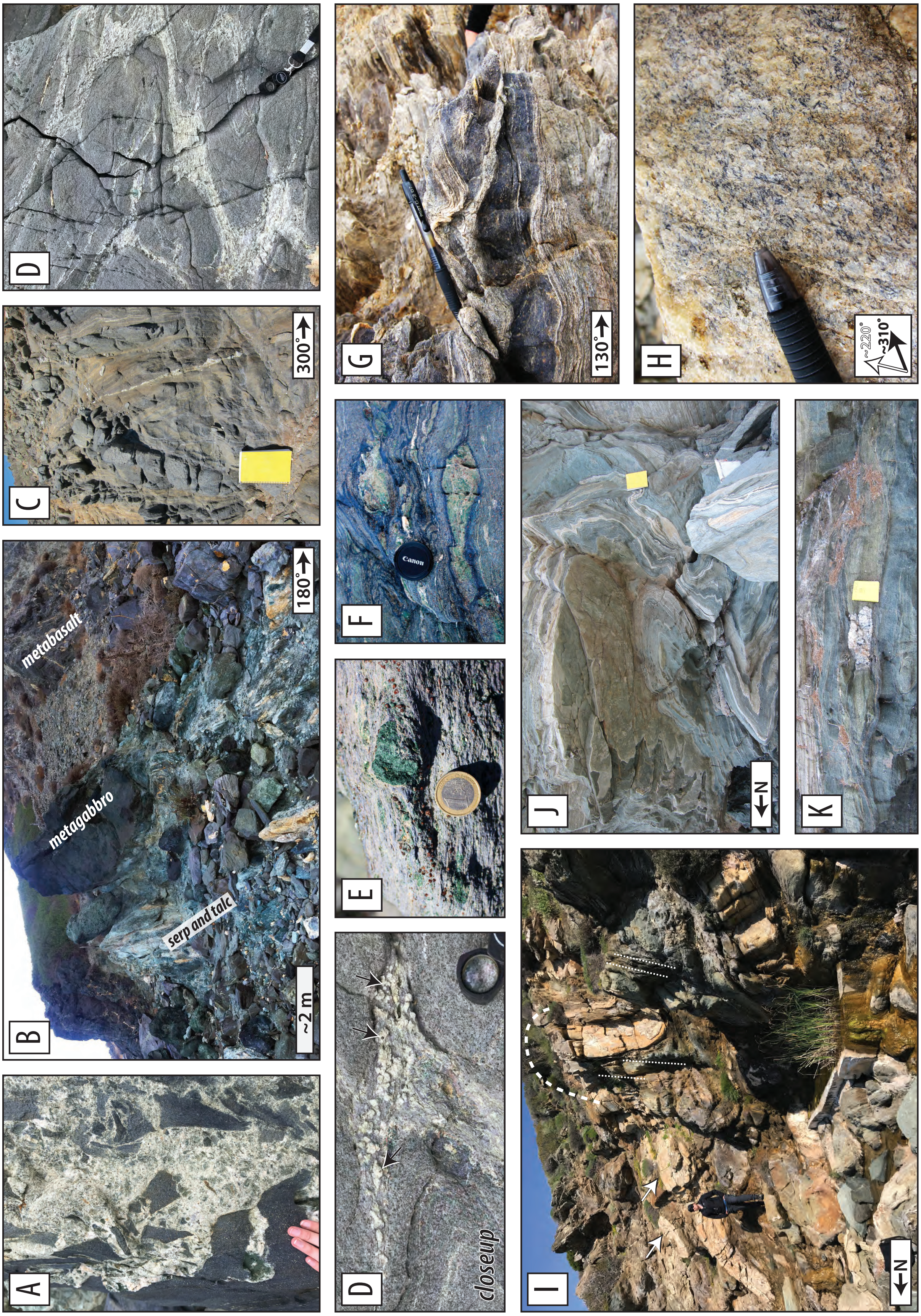

Figure 5: Caption next page.

Figure 5: (Previous page.) Selected field photos showing prograde (A,B,D) and retrograde (C,F-K) deformation and metamorphism. (A) Preservation of primary igneous breccias at Grizzas. (B) Right-side-up sequence of oceanic lithosphere at Kini. (C) Prograde foliations are folded into upright, open-to-tight folds with NE-SW-oriented hinge lines at Kalamisia during D_{T1}. (D,E) S_S at Kini contains lawsonite pseudomorphs and omphacite with glaucophane- and garnet-filled pressure shadows. Black arrows in the close-up photo of (D) point to pseudomorphs with garnet inclusions. (F) D_{T1} retrogression under blueschist-facies conditions is marked by local static glaucophane coronas formed around pinched eclogite lenses at Vaporia. (G,H) S_S is cut by S_{T1} crenulation cleavage at Azolimnos. (H) Two glaucophane lineations record transposition of S_S (black arrow, parallel to pen) into alignment with crenulation hinges (white arrow) during D_{T1}. (I-K) D_{T2} greenschist facies retrogression and upright folding at Delfini (I) and Lotos (J,K). (I) White arrows point to F_S folds along the limbs of F_T fold. Dashed white lines mark the axial planar S_T cleavage. (J) S_S cross-cut by D_T folding; fold axes trend E-W. (K) Coaxial, lineation-parallel D_{T2} brittle boudinage of epidote-rich lenses in greenschists.

lineations define great circles, likely reflecting folding of earlier (D_R) fabric during D_S (Fig. 4C, 4E; relicts at Azolimnos in Fig. 4J). In other localities, glaucophane lineations appear to be reoriented into moderately S- or SW-plunging clusters (e.g. Grizzas and Kini, Fig. 4B,E).

Centimeter-sized, prismatic pseudomorphs after lawsonite indicate that lawsonite grew at the culmination of D_S but did not survive peak conditions. Syn-to-post-kinematic blasts overgrow the mafic blueschist foliation at Grizzas and Lia, decorate foliation-parallel compositional layers at Kini (Fig. 5C), and commonly contain inclusions of garnet, and are included by garnet (Fig. 5D, closeup). Pseudomorphs are weakly attenuated along the limbs of folds, but preserve their diamond-like shapes in fold hinges (Fig. 5C,D).

4.2.2 D_S Microstructures and Mineral Chemistry

D_S micro-textures in meta-sedimentary rocks are characterized by strong quartz-mica cleavage-microlithon S_S fabrics and rotated inclusion trails in garnets that are mostly continuous with external foliations (Fig. 6C). Quartz-rich microlithons have strong lineation-parallel shape-preferred orientations, and mica-rich cleavages comprise intergrown phengite and paragonite (Fig. 6C, Fig. 7C). Lawsonite pseudomorphs preserved as inclusions in garnet comprise intergrown epidote and white mica, recording the up-temperature reaction *lawsonite = epidote + paragonite +* H_2O (Fig. 6D).

D_S micro-textures in mafic blueschists are characterized by compositional segregation defined by glaucophane-rich and epidote-rich layering alternating on the mm-scale (~50-200 μm grain size) (Fig. 6E). The S_S foliation contains syn-kinematic porphyroblasts of garnet and omphacite (~300 μm-5 mm), and rutile with minor titanite overgrowths (Figs. 6F, 7A). Syn-kinematic phengitic white mica is chemically homogeneous and has 3.35-3.45 Si atoms p.f.u. (Fig. B1). Omphacite and garnet deflect local foliations, and have pressure shadows and strain caps composed of glaucophane, phengite and paragonite, and/or more omphacite (Fig. 5E, 7A). Omphacite porphyroblasts in Kini blueschists have cores of low-Na, high-Mg omphacite, fringed by asymmetric, syn-kinematic pressure shadows of high-Na, low-Mg omphacite (Fig. 7A). D_S amphibole is glaucophane (Figs. 7A, 8A). Rare examples reveal glaucophane cores with thin, patchy rims (Fig. 7B) that trend towards lower $Al^{iv}/(Al^{iv}+Fe_{tot})$ values and higher $(Na+K)_A$ (Fig. 8A, Fig. B1).

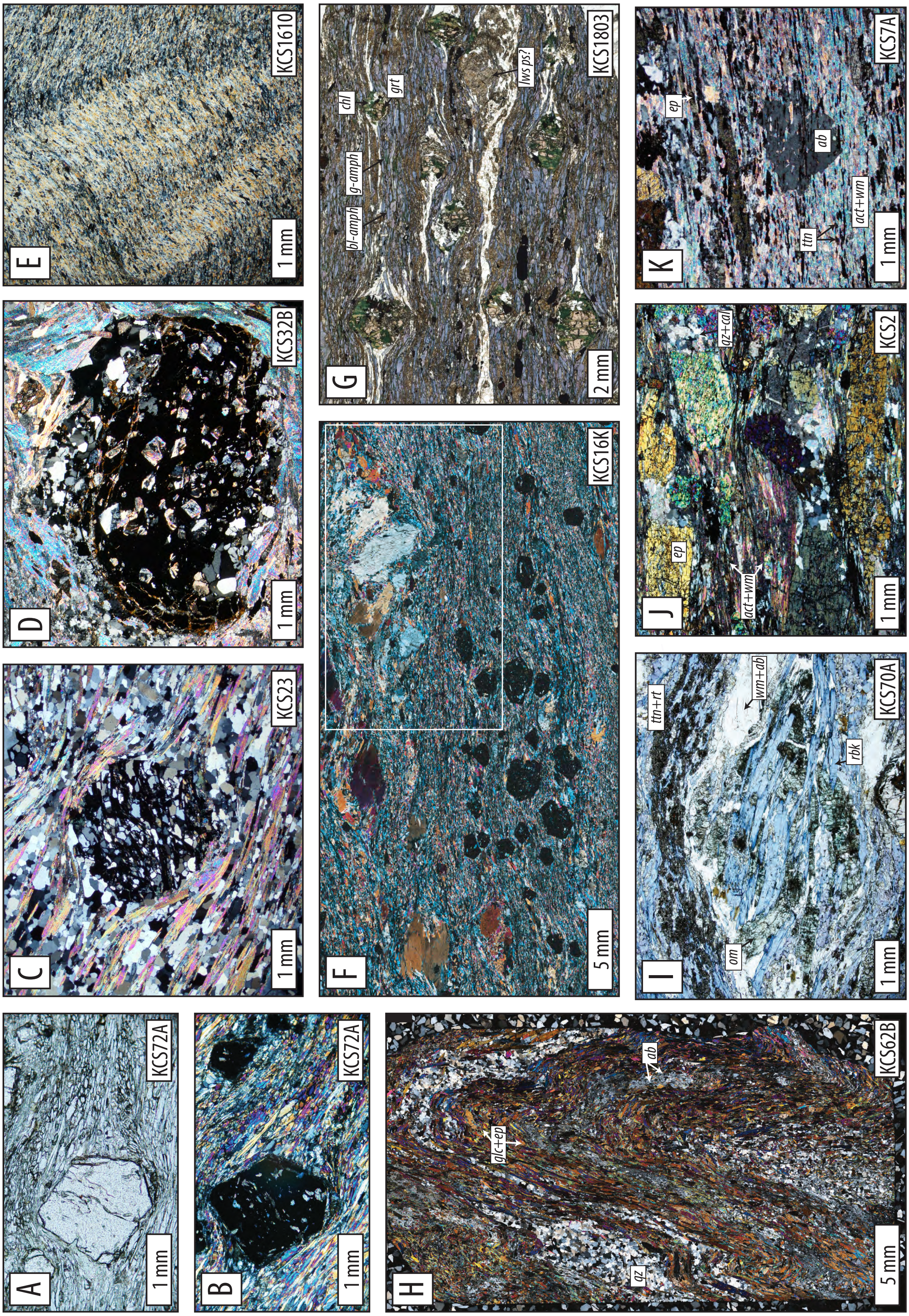

Figure 6: Caption next page.

Figure 6: (Previous page.) Selected photomicrographs showing prograde (A-F) and retrograde (E, G-K) deformation and metamorphism. (A,B) Internal S_R inclusion trails from Lia Beach (A, PPL; B, XPL). (C) S_S contains syn-kinematic garnet porphyroblasts with foamy quartz inclusion trails that are rotated but continuous with respect to the dominant external S_S foliation. (D) D_S garnets include pseudomorphs after lawsonite (comprising epidote and white mica). (E, F) S_S in mafic blueschists. (E) S_S is cut by D_{T1} crenulation under glaucophane-stable conditions in mafic blueschists. (F) Omphacite and garnet in D_S Kini blueschists have asymmetric pressure shadows filled with high-pressure minerals. (G-I) D_{T1} retrogression in bimodal meta-volcanics at Kampos (H), Azolimnos (H) and Kalamisia (I). (H) D_{T2} crenulation transposes S_S, and strengthens as albite, chlorite, and actinolite stabilize. (I) Omphacite and paragonite break down to epidote, blue amphibole, and albite. (J,K) D_{T2} in Lotos greenschists. (J) Brittle micro-boudinage of epidote porphyroblasts. (K) Final stages of D_{T2} are characterized by post-tectonic albite growth.

4.3 D_T – Retrograde fabric development, crenulation, and re-folding through blueschist-to-greenschist facies conditions

D_T represents retrograde deformation under blueschist-to-greenschist facies conditions during exhumation. D_T is distinguished by: (1) transposition of the S_S foliation during formation of upright, open to tight F_T folds and progressive new (S_T) fabric development; (2) lineation orientations that rotate from N-NE (D_{T1}) to E-W (D_{T2}) with progressive strain and (in general) increasing greenschist facies retrogression; (3) dominantly coaxial, but locally non-coaxial deformation; and (4) chemical zonations in amphibole tracking syn-kinematic decrease in pressure and temperature.

4.3.1 D_T Structures

D_{T1} captures incipient deformation and retrogression during exhumation, and is best recorded at Kampos Belt and Palos (Fig. 4A,C), Azolimnos (Fig. 4J), and Kalamisia (Fig. 4I), and locally at Kini (Fig. 4E). D_{T1} structures refold older S_S foliations into inclined-to-upright, open-to-tight, shallowly to moderately N- and NE-plunging folds (Fig. 4C, 4G,H, 4I,J; 5C)). Glaucophane, calcite, and quartz mineral and stretching lineations are oriented parallel to F_T fold hinge lines (Fig. 4C,I,J). Along Kampos Belt, D_{T1} fold axes span ∼335-055°/15-45°, with a cluster of moderately N-plunging folds (e.g. Fig. 4C). At Azolimnos, D_{T1} folding locally develops an upright crenulation cleavange (S_T) that cuts the S_S foliation (Fig. 4I,J; 5G). Cm-scale spaced cleavages are parasitic to larger open folds with 045°/5-10° fold axes and steep axial planes. At Azolimnos, glaucophane lineations define a great circle and swing from N to NE into alignment with F_{T1} crenulation hinge lines (Fig. 5H). Crenulation of Kini rocks is defined by a vertical, NE-striking S_{T1} cleavage that cross-cuts mafic blueschists (Fig. 4E).

D_{T2} captures E-W orientated mineral and stretching lineations that are primarily indicative of greenschist facies conditions (e.g., Lotos, Delfini; Fig. 4D,F) but locally preserve blueschist facies conditions where strain was highly non-coaxial (i.e., Fabrikas; Fig. 4K), and can be seen in a wide range of rock types throughout central and southern Syros. At Vaporia, the mafic blueschists and eclogites and the surrounding meta-sedimentary rocks develop identical D_{T2} structures (Fig. 4G,H). Single greenschist facies F_{T2} folds range in geometry from open to tight and have near-vertical, E-NE- to E-W striking axial planes. F_{T2} fold axes cluster strongly around ∼070-110°/5-30° (Figs. 4D,F; 5I,J), and mineral and stretching lineations defined by actinolite, quartz, calcite, and relict glaucophane are oriented parallel to F_{T2} hinge lines (Fig. 4D,F,H). Older S_S foliations are visible as S- and Z-folds (e.g. Fig. 5I,J) with hinge-limb layer thickness variations locally exceeding 20:1 (Fig.

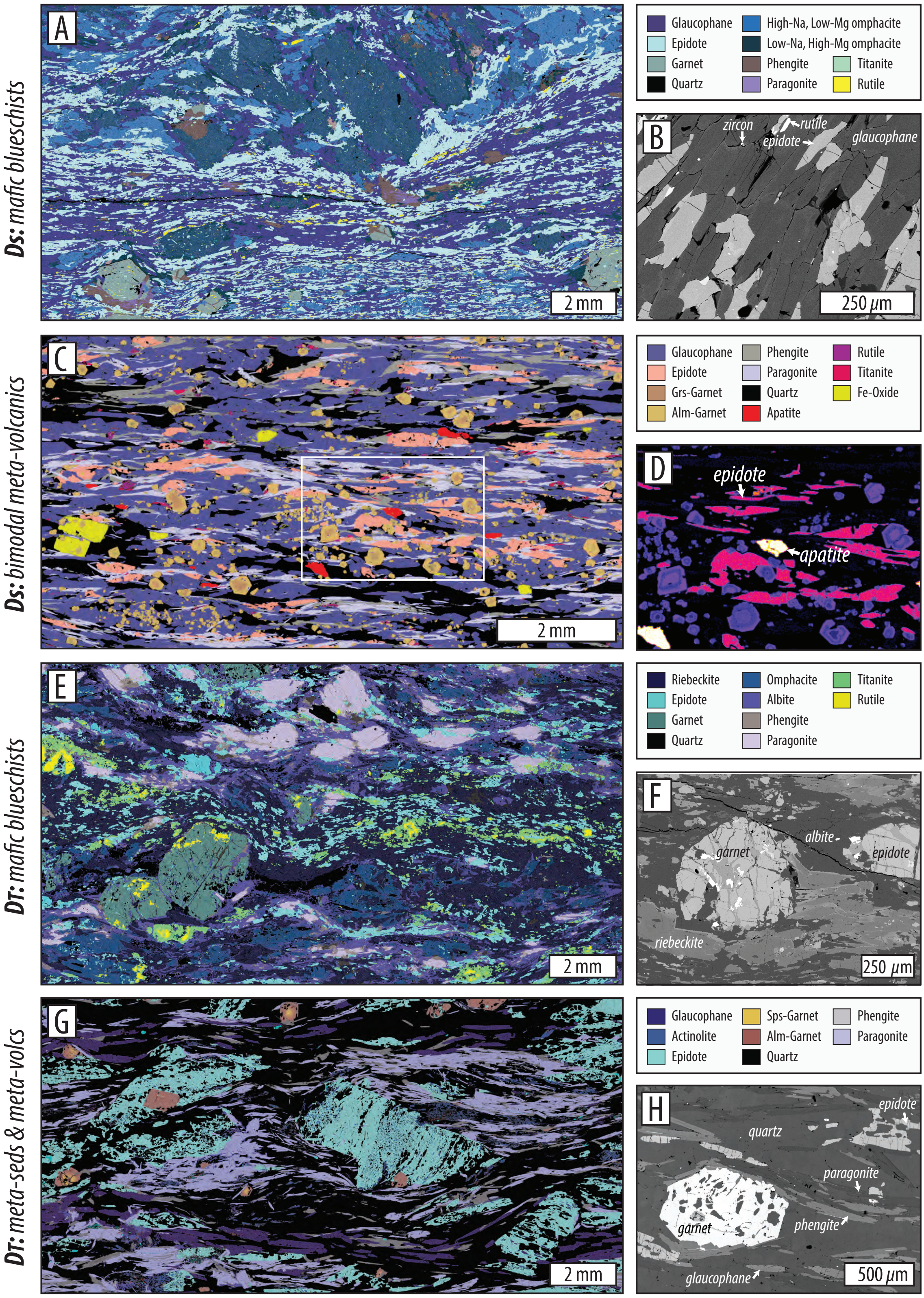

Figure 7: False-colored X-Ray maps and representative BSE images of D_S in Kini blueschists (A,B) and Azolimnos bimodal meta-volcanics (C,D), D_{T1} in Kalamisia blueschists (E,F), and D_{T2} in Fabrikas quartz-mica schists (G,H). Quantitative analyses of sodic amphiboles in (B, KCS53) and (F, KCS12B) are shown in Fig. 8; white mica analyses from (H, KCS65) are shown in Fig. B1.

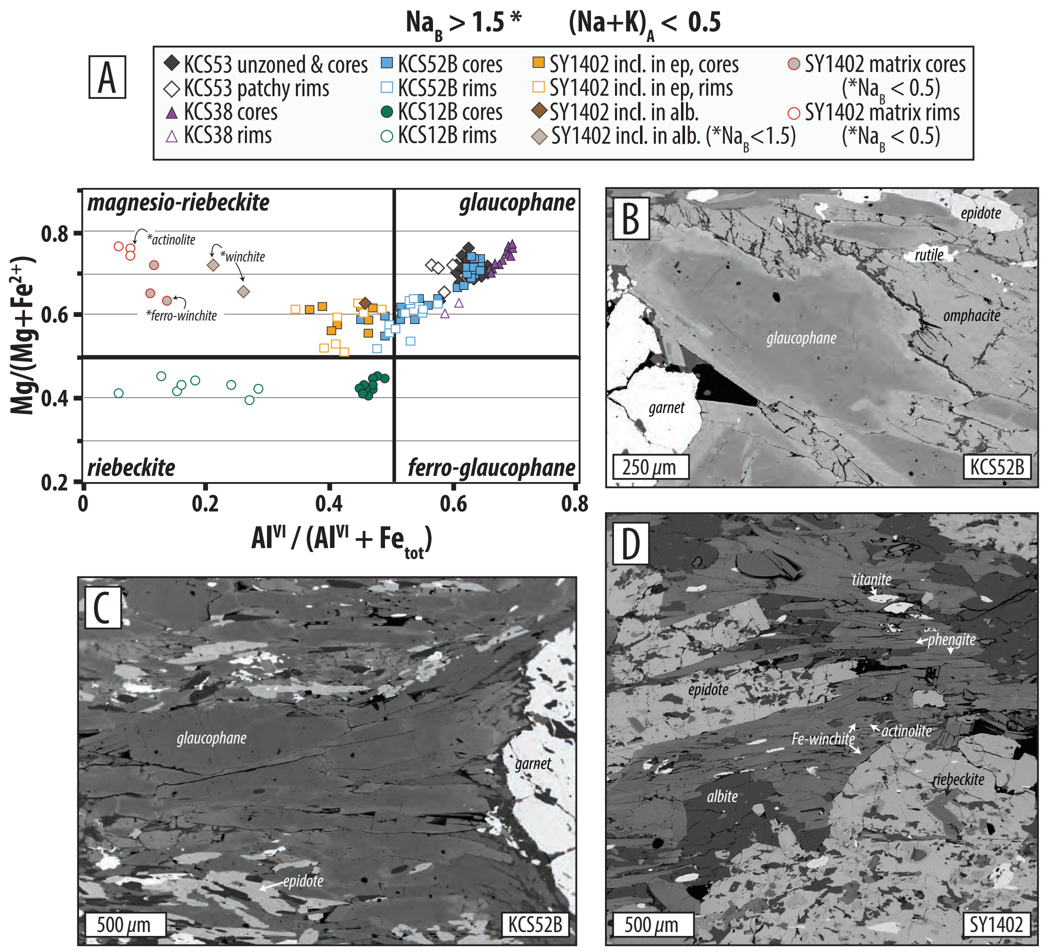

Figure 8: Amphibole mineral chemistry and micro-textures. (A) Quantitative amphibole EPMA analyses (Leake et al. (1997) classification scheme). All analyses have $Na_B > 1.5$ apfu except for those indicated with an asterisk. (B) D_{T1} static growth zonations in glaucophane contained in retrogressed eclogite pod. (C) D_{T1} lineation-parallel zonations developed in glaucophane-filled strain shadow fringing garnet porphyroclasts. (D) Greenschists preserve relict D_{T1} sodic amphibole as inclusions in epidote, and matrix amphibole records lineation-parallel compositional changes during D_{T2} retrogression.

C1). F_{T2} folds have axial planar cleavages decorated with actinolite, epidote, and chlorite. Coaxial stretching parallel to F_{T2} fold hinges is common, resulting in semi-brittle to brittle boudinage of epidote-rich lenses visible from the meso- to the micro-scale, as competent lithologies become brittle during exhumation (Fig. 5K).

Pulses of D_T metamorphism that are not associated with penetrative strain are seen at Vaporia where pinched eclogite pods are rimmed by roughly even-thickness inky blue coronas of glaucophane (Fig. 5F), and along Kampos Belt where the margins of meta-gabbros develop radiating clusters of blue and green amphibole needles (Fig. C1). Although D_T strain is primarily coaxial, strongly asymmetric strain occurs locally on the E-SE side of the island. Non-coaxial D_{T1-2} is best preserved at Kalamisia and Fabrikas, respectively. At Fabrikas for example, outcrop-scale extensional shear bands and boudinage cross-cut eclogite pods and are decorated by glaucophane (partially replaced by actinolite) and quartz (Kotowski & Behr, 2019).

4.3.2 D_T Microstructures and Mineral Chemistry

D_{T1} microstructures transpose and retrogress older S_S foliations, record geochemical evidence for retrogression from peak conditions through primarily blueschist facies conditions, and are primarily coaxial. Crenulation hinges that record D_{T1} in mafic blueschists are defined by high-Si white mica and glaucophane that has an identical composition to glaucophane defining the S_S foliation (Lia Beach, Fig. 6E; Fig. B1). Coaxial D_{T1} deformation in mafic blueschists is evidenced by symmetric strain shadows around partially chloritized garnets. During D_{T1}, S_S-defining blue amphibole grows in the symmetric strain shadows and records lineation-parallel growth zonations trending from glaucophane to magnesio-riebeckite (Vaporia, Fig. 8A,C) and locally becomes actinolitic (e.g. Kampos, Fig. 6G). Some static textures record the same compositional trend (e.g. Fig. 8A,B). At Kalamisia, extensional C-C' fabrics are well-developed in thin section, and C' top-to-the-ENE shear bands are decorated with albite, paragonite, and phengite (Fig. 7E,F). C' cleavages are also defined by finely recrystallized blue amphibole that records lineation-parallel core-to-rim zonations from high-Al riebeckite to low-Al (and lower $(Na+K)_A$) riebeckite (Figs. 6I, 7F, 8A). Omphacite and paragonite porphyroblasts record the breakdown reaction *omphacite + paragonite +* H_2O *= sodic amphibole + epidote + albite* (Fig. 6I), and rutile is overgrown by syn-kinematic titanite (Figs. 7E). In quartz-mica schists, the retrogressed S_S foliation comprises alternating glaucophane-rich and quartz-mica $\pm$ albite-calcite layering; the syn-D_{T1} axial planar cleavage, S_{T1}, is defined by actinolite, albite, phengite and paragonite in the cores of upright F_{T1} folds (Fig. 6H).

D_{T2} microstructures transpose and retrogress older S_S foliations, and are primarily coaxial and record geochemical evidence for retrogression under greenschist facies conditions (e.g. Delfini and Lotos). Locally D_{T2} was non-coaxial and developed under blueschist facies conditions (e.g. Fabrikas). Mafic greenschists that record D_{T2} comprise strongly retrogressed S_S foliations that are defined by fine-grained white mica, albite, epidote, actinolite, chlorite, calcite, and titanite ($\sim$50-500 μm grain size), and contain lineation-parallel epidote porphyroblasts ($\sim$2-5 mm) and unoriented, mat-like albite porphyroblasts ($\sim$1-5 mm) (Fig. 6J,K). Amphibole occurs in two distinct contexts: as inclusions in epidote and albite porphyroblasts, and as a dominant S_S foliation-forming phase. Amphibole inclusions record core-rim zonations evolving from magnesio-riebeckite to winchite, and matrix amphibole record core-rim zonations evolving from ferro-winchite to actinolite (Figs. 8A,D). S_S-defining, syn-D_{T2} epidote porphyroblasts have pressure shadows filled with white mica, calcite and albite, and are boudinaged, with necks filled by quartz and calcite (Fig. 6J, 8D). In blueschist facies fabrics at Fabrikas, the retrogressed S_S foliation comprises syn-D_{T2} epidote porphyroblasts that contain rotated inclusion trails of quartz and glaucophane and inclusions of garnet that preserve syn-D_S spessartine-to-almandine zonations (Figs. 7G,H). Phengite and paragonite define C- and C'-planes of an extensional, top-to-the-E shear fabric. Phengitic white mica reveals a tight range of Si atoms p.f.u. ($\sim$3.33-3.39 a.p.f.u, Fig. B1), and Si content of C- and C'-defining phengite is identical (Fig. 7G, Fig. B1). Lineation-parallel brittle micro-boudinage of epidote and amphibole porphyroblasts is common; epidote boudin necks are filled with quartz, and blue amphibole boudin necks contain green amphibole needles. A planar S_{T2} fabric that cuts S_S is only found in the core of F_{T2} folds (i.e. S_{T2} crenulation cleavage at Delfini, Cisneros et al. (submitted)).

5 Synthesis of P-T Conditions for Each Deformation Stage

5.1 D_R P-T conditions

We interpret the D_R fabric in the CBU to have passed through lawsonite-blueschist facies conditions based on several lines of evidence, including: (1) D_R inclusion trail mineralogy (e.g. glaucophane, omphacite, phengite); (2) pseudomorphs of D_{R-S} lawsonite included in D_S garnets from meta-basites on Syros (also seen on Sifnos) (Ridley, 1982; Okrusch & Bröcker, 1990); and (3) syn-kinematic D_{R-S} omphacite blasts recording up-pressure, core-

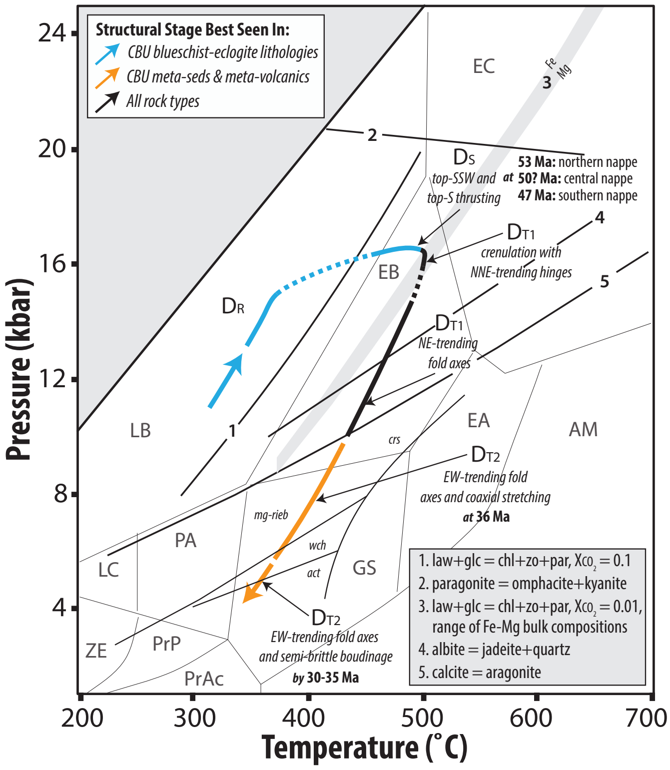

Figure 9: Preferred P-T-D-t path for the CBU, consistent with observations and analytical results from this study. The shape of the path is modified from (Schumacher et al., 2008). Amphibole stability fields constraining D$_{T2}$ temperatures are from Otsuki and Banno (1990). Mineral abbreviations: crs = crossite (sodic amphibole), mg-rieb = magnesio-riebeckite, wch = winchite, act = actinolite. Facies fields defined in Figure 3.

to-rim zonations marked by increasing jadeite component (Fig. 7A) (cf. Thompson, 1974). Lawsonite and epidote appear to have both been stable in mafic bulk compositions during D$_R$, with lawsonite growing later on the prograde path under higher-pressure conditions (cf. Ballevre et al., 2003). This is consistent with textural observations of lawsonite growing late, syn- and post-tectonic with respect to the S$_R$ foliation, incorporating inclusions of garnet (which also grows near peak pressures, cf. Dragovic et al. (2012); Baxter and Caddick (2013); Dragovic et al. (2015)), and being included by garnet.

5.2 D$_S$ P-T conditions

Peak P-T conditions for the D$_S$ deformation fabric are justified as follows: Peak temperatures have been calculated from garnet-omphacite major element exchange for mafic blueschists and eclogites (450-500°C) (Schliestedt, 1986; Okrusch & Bröcker, 1990; Rosenbaum et al., 2002); the upper limit of glaucophane stability in marble (∼500°C at ∼15-16 kbar; Schumacher et al. (2008)); and calculated lawsonite-out reaction lines (∼400-500°C over ∼12-20 kbar, depending on bulk rock and fluid composition) (Liou, 1971; Evans, 1990; Schumacher et al., 2008) (Fig. 9). Raman Spectroscopy of Carbonaceous Material from graphite schists suggests slightly higher temperatures of ∼540-560°C (Laurent et al., 2018).

Reported peak pressures for D$_S$ are variable in the literature, and challenging to reconcile. Early conventional thermobarometry suggested peak P of ∼12-18 kbar in mafic blueschists and eclogites (Dixon, 1976; Schliestedt, 1986; Okrusch et al., 1978; Okrusch & Bröcker, 1990). These pressures are supported by recent solid inclusion quartz-in-garnet barometry constraining garnet growth at Kini, Kalamisia, Delfini, and Lotos to ∼13-17 kbar (Behr et al., 2018; Cisneros et al., submitted). However, more recent thermodynamic modeling accounting for garnet fractionation suggests rocks reached ∼20-24 kbar (Trotet et al., 2001a; Laurent et al., 2018; Skelton et al., 2019). We consider this unlikely based on the abundance of S_S paragonite and absence of kyanite in meta-mafic rocks, which suggests that the upper stability limit of paragonite at ∼20-23 kbar was not reached (Schliestedt, 1986; Okrusch & Bröcker, 1990; Skelton et al., 2019) (Fig. 9). Large differences in P-T estimates between traditional phase equilibria and recent thermodynamic modeling may reflect arbitrary choices of thin section domains selected as representative bulk compositions (e.g. Lanari & Engi, 2017). This is especially likely in garnet-bearing lithologies, due to the strong disequilibrium effect that garnet exerts on local bulk composition (Lanari et al., 2017; Lanari & Engi, 2017; Lanari & Duesterhoeft, 2018). It is also possible that higher-P conditions are real, but have not yet been sampled by solid inclusion techniques or traditional phase equilibria.

5.3 D_T P-T conditions

During D_T, foliation-forming amphiboles transition from glaucophane to (magnesio) riebeckite, to winchite, to actinolite. The progressive decrease of total Al, Na_B, and $(Na+K)_A$ in amphibole indicates that P and T decreased as D_T evolved. Glaucophane coronas that develop around eclogite pods during D_{T1} are chemically similar to syn-D_S glaucophane, and retrogressed glaucophane records decreasing Al^{vi} (KCS53, KCS52B) and Na_B (KCS53) from core to rim, and a minor increase in $(Na+K)_A$ as (Fig. 8, Fig. B1). These signatures indicate decompression and potentially slight warming (Raase, 1974; Laird & Albee, 1981; Robinson, 1982; Moody et al., 1983; Ernst & Liu, 1998), at the subduction-to-exhumation transition.

D_{T2} is characterized by foliation-forming calcic amphiboles, and local relicts of sodic amphiboles are found as inclusions in porphyroblasts. The transition from sodic-to-calcic amphibole recorded here indicates cooling during decompression (Thompson, 1974; Brown, 1977; Laird & Albee, 1981; Moody et al., 1983; Maruyama et al., 1983; Otsuki & Banno, 1990; Schmidt, 1992; Ernst & Liu, 1998) through albite-epidote blueschist facies and eventually greenschist facies conditions (Fig. 9). This P-T trend is supported by the abundance of albite and titanite overgrowths on rutile, and boudin neck quartz-calcite oxygen isotope temperatures and quartz-in-epidote inclusion barometry presented by Cisneros et al. (submitted). We have not observed amphibole chemistry that supports isothermal decompression nor a positive thermal excursion into the epidote-amphibolite facies field (e.g. edenite, pargasite, crossite), as suggested by Trotet et al. (2001a), Lister and Forster (2016), and Laurent et al. (2018) P-T-D paths.

6 Geochronology

6.1 New multi-mineral Rb-Sr isochron petrochronology

Multi-mineral Rb-Sr Isochron Geochronology has been applied to exhumed HP/LT metamorphic rocks for dating deformation and metamorphism with great success (Freeman et al., 1997; Glodny et al., 2005; Ring et al., 2007; Glodny et al., 2008; Kirchner et al., 2016; Angiboust et al., 2016; Cliff et al., 2016). The primary assumption required to construct a multi-mineral isochron is that the phases defining the isochron were co-genetic, so they all inherited the same initial Sr composition. We separated and picked minerals that we hypothesized were co-genetic based on structural and microstructural arguments posed above, and quantitatively tested this hypothesis by identifying phases that were in isotopic disequilibrium (i.e. fell off the isochron) (Cliff & Meffan-Main, 2003). Strong foliations support the assumption of syn-kinematic recrystallization of selected minerals, which can reset the Sr isotopic signature between mica and co-genetic phases to temperatures as low as 300°C (Müller et al., 1999). Furthermore, diffusional resetting of the Rb-Sr system is thought to begin at ∼550-600°C (Inger & Cliff, 1994; Glodny et al., 2008), which exceeds maximum temperatures in the CBU. Therefore, we consider our Rb-Sr ages reported herein are interpreted as (re-)crystallization ages associated with deformation.

Following Glodny et al. (2003, 2008), we used a bulk mineral separation technique and cut out ∼5 cm^3 cubes of rock from hand samples to isolate specific fabrics (one D_S, one D_{T1} and three D_{T2}). Samples were crushed with a small hammer between sheets of paper, ground gently with a rock crusher, and sieved and separated by grain size. Grain size fractions 125-250 μm and 250-500μm were frantzed to separate minerals based on magnetic susceptibility. Mineral separates were picked by hand under a microscope, and white mica separates were cleaned of inclusions by gently smearing them in a mortar and pestle and washing them through a sieve with ethanol. All Rb and Sr isotopic separation and analyses were done at the University of Texas at Austin in the Radiogenic Isotopic Clean Lab. All separates (except apatite) were cleaned in 2 N HCl to remove surficial contamination and spiked with mixed high Rb/Sr and low Rb/Sr spikes. We followed methodology for mineral dissolution, isotope column chemistry, Thermal Ionization Mass Spectrometry (Sr analyses), Solution Inductively Coupled Plasma Mass Spectrometry (Rb analyses), and estimating uncertainties in isotopic ratios as described in Kirchner et al. (2016). Reproducibility on replicate USGS Standard Hawaiian Basalt (BHVO) Rb measurements determine the uncertainty of the Rb-Sr ratio, and long-term reproducibility on the NBS987 Sr standard determines the uncertainty of the Sr ratio (Table 2). Ages were calculated using the IsoplotR toolbox (Vermeesch, 2018) with the ^{87}Rb decay constant of $1.3972 \pm 0.0045 \times 10^{-11}$ per year (Villa et al., 2015).

6.1.1 Results

All of the isochrons described herein have Mean Standard Weighted Deviations (MSWDs) greater than 1, which suggests that the data dispersion exceeds that predicted by analytical uncertainties (i.e., the data are overdispersed) (cf. Wendt & Carl, 1991). However, MSWDs are a reflection of analytical precision (e.g. Kullerud, 1991; Powell et al., 2002), and reflect the goodness of fit of a regression line to the datapoints, which includes their analytical uncertainties. Our dataset has a very high analytical precision (calculated from reproducibility of standards measurements), which leads to a significant increase in the MSWD of a Rb-Sr isochron when the regression line does pass through a datapoint's uncertainties (e.g. Fig. 10B). However, we consider our Rb-Sr ages reliable records of true deformation and metamorphism events, after closer evaluation of our isochrons (see Table A1), despite their high MSWDs. This is because the isochrons were contructed from mineral suites that our structural and petrographic observations suggest are co-genetic, and the co-linearity of the data are striking (with some justifiable exceptions discussed below). The high MSWD values may reflect underestimation of our analytical uncertainties, or minor Rb-Sr disequilibrium during metamorphism (perhaps due to incomplete recrystallization, e.g. Halama et al. (2018)) that does not significantly affect our Rb-Sr ages (Table A1).

Sample SY1616 is an omphacite-blueschist collected at Kini Beach and records D_S (texturally identical to Fig. 7A). This sample yielded an age of 53.48 ± 0.65 Ma (MSWD = 5) based on a 10-point isochron defined by epidote, glaucophane, omphacite, five paragonite separates, garnet, and one phengite separate (Table 2, Fig. 10). To test the robustness of the isochron, several two- to five-point isochrons were calculated from combinations of the co-genetic phases; the age does not change but the MSWD is reduced (=1 for 2-pt isochrons by definition; <1 for 3- and 4-pt, and 1.4-1.7 for 5-pt).

Sample KCS1617 is a bimodal meta-volcanic schist collected at Azolimnos and records D_{T1} (similar to sample in Fig. 7C). This sample yielded an age of 45.51 ± 0.29 Ma (MSWD = 8) based on a 7-point isochron defined by glaucophane, four paragonite separates, and

Sample ID and Summary	Mineral	Rb (ppm)	Sr (ppm)	87Rb / 86Sr	± 2σ	87Sr / 86Sr	± 2σ
SY1616: Kini omphacite-epidote blueschist	epidote (L18-001)	0.12	1008	0.00035	1.73E-07	0.703224	1.41E-05
Solution on 10 points: 53.48 ± 0.65 Ma	glaucophane (L18-010)	0.15	143	0.00301	1.50E-06	0.703225	1.41E-05
Initial 87/86 Sr: 0.703211 ± 0.000012	omphacite (L19-099)	0.28	31	0.02571	1.29E-05	0.703235	1.41E-05
MSWD = 5	paragonite (L19-097)	0.31	19	0.04765	2.38E-05	0.703244	1.41E-05
	paragonite (L19-093)	0.31	16	0.05829	2.91E-05	0.703234	1.41E-05
	paragonite, 0.5 A, 125-250 μm (L19-009)	0.37	17	0.06439	3.22E-05	0.703284	1.41E-05
	garnet #1 (L18-011)	0.29	13	0.06562	3.28E-05	0.703261	2.04E-05
	paragonite (L19-094)	1	44	0.07644	3.82E-05	0.703248	1.41E-05
	paragonite (L19-096)	6	142	0.12305	6.15E-05	0.703289	1.41E-05
	phengite, 0.4 A, 250-500 μm (L19-095)	35	24	4.26296	2.13E-03	0.706398	1.41E-05
	removed from isochron						
	garnet #2 (L19-098)	0.35	12	0.08338	4.17E-05	0.703353	1.41E-05
KCS1617: Azolimnos glaucophane-mica blueschist	paragonite (L19-103)	9	199	0.13309	6.65E-05	0.706681	1.41E-05
Solution on 7 points: 45.51 ± 0.29 Ma	paragonite (L19-102)	15	179	0.23810	1.19E-04	0.706776	1.41E-05
Initial 87/86 Sr: 0.706592 + 0.000022	glaucophane (L18-002)	0.3	3	0.33478	1.67E-04	0.706783	1.41E-05
MSWD = 8	paragonite (L19-100)	34	178	0.55161	2.76E-04	0.706927	1.41E-05
	paragonite, 0.8 A, 125-250 μm (L18-007)	5	14	0.97194	4.86E-04	0.707200	1.41E-05
	phengite (L19-101)	112	112	2.87985	1.44E-03	0.708433	1.42E-05
	phengite, 0.7 A, 250-500 μm (L18-005)	219	43	14.89794	7.45E-03	0.716067	1.43E-05
	removed from isochron						
	epidote (L18-003)	0.7	1486	0.00136	6.82E-07	0.706668	1.41E-05
	garnet #1 (L19-004)	0.69	8	0.26530	1.33E-04	0.706583	1.41E-05
	garnet #2 (L19-104)	0.87	4	0.63469	3.17E-04	0.706733	1.41E-05
KCS1621: Delfini actinolite-mica greenschist	epidote	1	1961	0.00143	5.71E-07	0.706597	1.41E-05
Solution on 7 points: 37.06 ± 0.12 Ma	paragonite, 0.6 A, 250-500 μm (L19-225)	54	258	0.60594	2.42E-04	0.706951	1.41E-05
Initial 87/86 Sr: 0.706626 + 0.000033	paragonite, 0.5 A, 125-250 μm (L19-222)	326	39	2.37806	9.51E-04	0.707878	1.42E-05
MSWD = 13	chlorite, 0.25 A, 250-500 μm (L19-226)	9	11	2.41488	9.66E-04	0.707852	1.42E-05
	paragonite, 0.6 A, 125-250 μm (L19-224)	150	155	2.79655	1.12E-03	0.708052	1.42E-05
	phengite, 0.5 A 125-250 μm (L19-223)	142	173	24.45665	9.78E-03	0.719330	1.44E-05
	phengite, 0.4 A, 250-500 μm (L19-221)	369	21	51.64803	2.07E-02	0.733354	1.47E-05
	removed from isochron						
	phengite, 0.4 A, 125-250 μm (L19-220)	343	47	21.16233	8.46E-03	0.717173	1.43E-05
SY1644: Delfini mineralization in epidosite boudin neck	epidote (L19-041)	0.23	2170	0.00031	1.23E-07	0.706608	1.41E-05
Solution on 3 points: 36.05 ± 2.6 Ma	actinolite (L19-042)	17	123	0.39700	1.59E-04	0.706899	1.41E-05
Initial 87/86 Sr: 0.706655 + 0.00058	white mica (L19-040)	303	30	29.24565	1.17E-02	0.721388	1.44E-05
MSWD = 82							
SY1402: Lotos reaction rim around epidosite pod	apatite	2	726	0.00992	5.21E-03	0.70497	8.10E-06
Solution on 5 points: 34.88 ± 5.8 Ma	white mica < 125 μm (L19-029)	204	13	47.20997	1.89E-02	0.72438	1.45E-05
Initial 87/86 Sr: 0.70455 ± 0.00363	white mica 125-250 μm (L19-030)	227	10	68.82184	2.75E-02	0.73953	1.48E-05
MSWD = 76000	white mica, 0.4 A, 250-500 μm (L19-031)	234	7	95.01809	3.80E-02	0.75342	1.51E-05
	white mica, 0.6 A, 250-500 μm (L19-032)	203	9	67.84958	2.71E-02	0.73643	1.47E-05

Table 2: Summary of Rb and Sr concentrations and measured ratios from analyzed samples. Mineral separates discarded from calculated isochrons are listed. Uncertainty in age estimate (i.e. $\pm t$) are calculated assuming overdispersion, as z = y x $\sqrt{MSWD}$, where y is the confidence interval for t using the appropriate number of degrees of freedom.

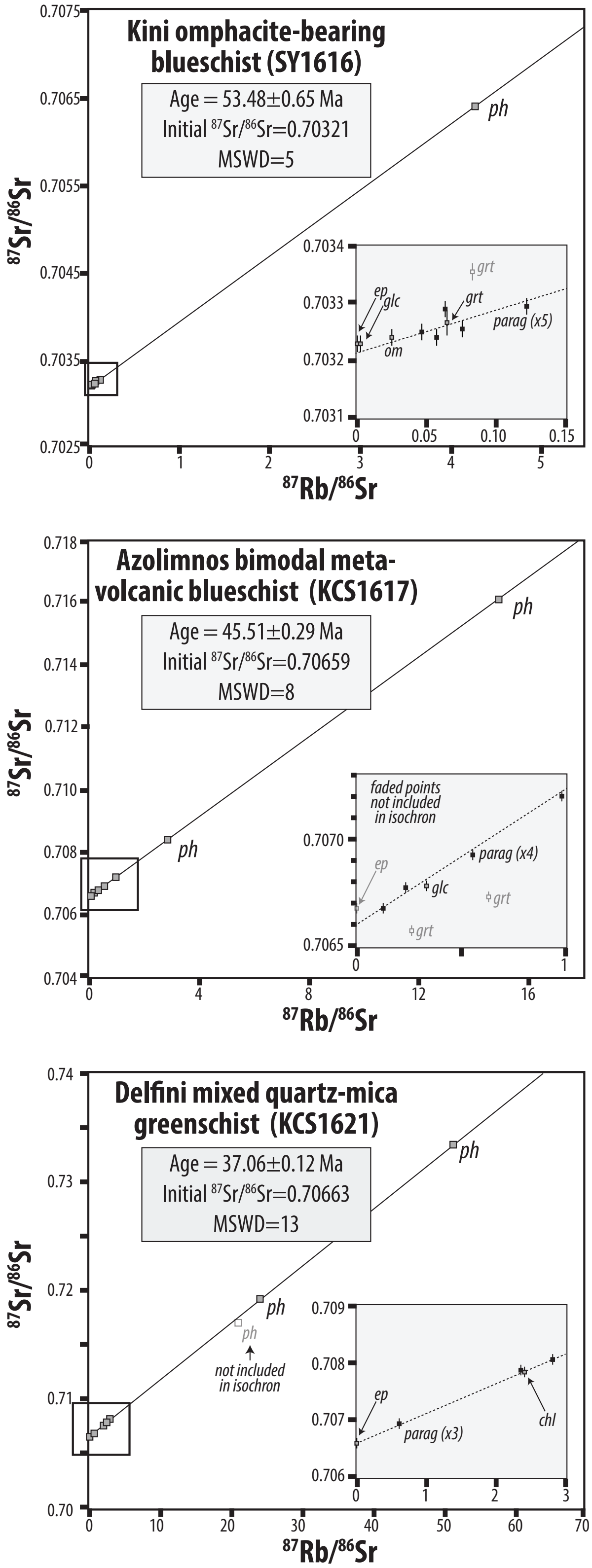

Figure 10: Multi-mineral Rb-Sr isochrons from a Kini omphacite-blueschist (SY1616), Azolimnos quartz-mica blueschist (KCS1617), and Delfini quartz-mica greenschist (KCS1621). Grey insets are zoom-ins of low Rb/Sr separates outlined in black boxes. Faded grey symbols were excluded from isochron calculations. Multiple paragonite separates for each isochron are shown in black symbols. Sample SY1616 records D_S in the northern nappe, KCS1617 records D_{T1} in the central nappe, and KCS1621 records D_{T2} in the central nappe. D_T retrogression pre-dates the onset of regional core complex capture. Mineral abbreviations: ep = epidote, glc = glaucophane, om = omphacite, grt = garnet, parag = paragonite, ph = phengite, chl = chlorite.

two phengite separates (Table 2, Fig. 10). Two garnet separates fell off of the isochron and are discarded in the age calculation. We justify this based on microstructural observations shown in Figure 7D; garnets preserve complex Ca-zonation patterns and may record pulsed growth. Furthermore, garnets are D_S porphyroblasts and are not expected to be in isotopic equilibrium with the D_{T1} fabric during incipient retrogression. Adding epidote to the isochron does not change the age (45.43 ± 0.46 Ma, n=8), but increases the MSWD to 23. Epidote is stable throughout subduction and exhumation and could record subtle zonations that grew during subsequent deformation events and therefore may not be co-genetic (e.g. Cisneros et al., submitted).

Sample KCS1621 is a quartz-mica schist collected from Delfini and records D_{T2} in meta-sedimentary schists. It was collected from a fold limb of a structure like the one in Fig. 5I, and is interlayered with quartz-schists on the decimeter-scale that locally preserve blue amphibole lineations. This sample yielded an age of 37.06 ± 0.12 Ma (MSWD = 13) based on a 7-point isochron defined by epidote, chlorite, 3 paragonite separates, and 2 phengite separates (Table 2, Fig. 10). For this sample, various combinations of 2- to 6-pt isochrons all yield ages of ∼35-37 Ma with MSWD varying from $<<$ 1 (e.g. 3-pt epidote-chlorite-paragonite), to 1 (e.g. 2-pt paragonite-chlorite) to 21 (e.g. 4-pt epidote-chlorite-phengite-phengite). Even the isochrons that are not defined in high-Rb space (i.e. do not contain phengite) yield nearly identical ages to the 7-point isochron (Table A1).

Sample SY1644 is a collection of minerals precipitated in the neck of a brittlely-boudinaged epidote-rich lens from Delfini, and sample SY1402 is a greenschist facies reaction rind at the margin of an epidote-rich lens from Lotos. These samples are representative of semi-brittle boudinage associated with D_{T2} stretching (e.g. Fig. 5K). These samples yield ages with reasonable uncertainties, but extremely high MSWDs. Sample SY1644 yielded an age of 36.1 ± 2.6 Ma (MSWD = 82) based on a 3-point isochron defined by epidote, actinolite, and phengite, and sample SY1402 yielded an age of 34.9 ± 5.8 Ma (MSWD = 76000) based on a 5-point isochron defined by apatite and 4 phengites (Table 2). For both samples, 2-pt isochrons yield ∼36 Ma and ∼29-36 Ma, respectively (MSWD=1; Table A1). We consider these data qualitative, but these ages are similar to and trend slightly younger than KCS1621, which is consistent with our structural observations.

6.2 Synthesis of previously published metamorphic geochronology

We compiled all available metamorphic geochronology (to our knowledge, from 1987 through 2019) for Syros to date, and took inventory of the descriptions of deformation fabrics and metamorphic textures provided by the authors, to re-evaluate the significance of Eocene ages in the context of subduction vs. exhumation. We applied several qualitative filters to the dataset to derive a subset of ages that we can confidently attribute to fabric-forming events. The filters are justified as follows:

Zircon U-Pb ages are robust records of igneous crystallization, but as metamorphic ages, can be difficult to place in pro- or retrograde context (Tomaschek et al., 2003; Liu et al., 2006; Yakymchuk et al., 2017). We include U-Pb ages from Tomaschek et al. (2003) for comparison with other ages, but we do not rely on it for island-scale interpretations. *Garnet Lu-Hf and Sm-Nd* are considered reliable indicators of 'peak' subduction ages (i.e., maximum depths) (Lagos et al., 2007; Kendall, 2016), because HP/LT garnets tend to grow rapidly following reaction overstepping (Dragovic et al., 2012; Baxter & Caddick, 2013; Dragovic et al., 2015). *White mica Ar/Ar* has potential to capture timing of metamorphism during fabric development. However, this system is highly susceptible to disequilibrium, partial (re-)crystallization and mixed ages, and/or unpredictable loss or gain of radiogenic products, making it difficult to interpret the geological significance of an age (Maluski et al., 1987; Bröcker et al., 2013; Lister & Forster, 2016; Laurent et al., 2016). For the final dataset, we only included five Ar/Ar step-heating ages with strong plateaus from micro-drilled grains, one 10-pt inverse isochron derived from in-situ analyses, which all had clear micro-textural context (Laurent et al., 2017), and one strong plateau age from a well-characterized marble shear zone (Rogowitz et al., 2015). *Rb-Sr isochrons* are considered good indicators of fabric ages when the selected fabrics, and minerals defining them, are well-characterized by respective authors (Bröcker & Enders, 2001; Bröcker et al., 2013; Skelton et al., 2019). Micro-drilling of white micas and co-genetic Sr-rich phases (epidote or calcite) also provide strong textural context for regressed ages (Cliff et al., 2016).

In some cases, we propose different interpretations of published data based on our own structural observations. Skelton et al. (2019), for example, interpreted three of their Rb-Sr isochrons from Fabrikas as peak metamorphic ages (i.e., D_S), but we interpret Fabrikas fabrics to relate to D_{T1-2}, associated with early exhumation (cf. Fig. 4K,L).Cliff et al. (2016) analyzed micro-drilled phengites from blueschist-to-greenschist facies (i.e., D_{T1} to D_{T2}) extensional fabrics in calc-schists and quartz-mica schists. Four of their samples from Delfini were described as blueschist-facies (black stars in Fig. 11); however, our observations point to penetrative greenschist facies deformation at Delfini (D_{T2}). Glaucophane is locally preserved in abundance in calc-schists at Delfini, and elsewhere on Syros. Rather than reflecting blueschist facies conditions during deformation, this may be due to a glaucophane-stabilizing, CO_2-bearing fluid under greenschist facies P-T conditions (Kleine et al., 2014). Finally, Rogowitz et al. (2015) dated phengites from a top-E extensional greenschist facies marble shear zone, and hypothesized the ages would be Miocene in accordance with the regional 'M2'. They interpreted their Eocene ages as evidence that Miocene deformation did not reset the isotopic signature. However, our results suggest their ages capture a true Eocene recrystallization event (e.g. strong E-W stretching during greenschist facies D_{T2}).

In Figure 11, the refined compilation (n=44) and new Rb-Sr geochronology (n=5) are projected onto the cross-section line drawn in Figure 2. Where possible, ages are labeled according to fabric generation. Faded data points were assigned textural identities but do not record penetrative strain (e.g. randomly oriented, radiating cluster). Key observations from new and compiled geochronology include:

1. D_S, blueschist-to-eclogite facies deformation-metamorphism spans ∼53 to ∼47 Ma, and is captured by a multi-mineral Rb-Sr isochron (this study, Kini), Lu-Hf and Sm-Nd garnet ages, and an Ar/Ar white mica age from glaucophane-bearing eclogites.
2. D_S ages are oldest and well-clustered at Grizzas and Kini (∼53-52 Ma), and younger and potentially more widespread at Fabrikas (∼50-44 Ma).
3. D_{T1}, retrograde blueschist facies deformation-metamorphism spans ∼50-40 Ma (Rb-Sr isochrons and Ar/Ar single grain analyses) and youngs with structural depth, i.e. from Kampos, to Azolimnos, to Fabrikas.
4. D_{T2}, retrograde greenschist facies deformation-metamorphism spans ∼42-20 Ma (all Rb-Sr) and youngs with structural depth, i.e. from Palos (∼43-35 Ma), to Delfini (∼35-28 Ma), to Posidonia (∼28-20 Ma)
5. Rocks that presently occupy different structural levels developed distinct fabric generations contemporaneously. Examples include: Fabrikas D_S and Kampos D_{T1} (∼50-45 Ma), Fabrikas D_{T1} and Palos D_{T2} (∼43-38 Ma), and Posidonia D_{T2} and non-penetrative greenschist metamorphism in the north (faded symbols, ∼25-20 Ma).

7 A new tectonic model for the CBU on Syros

Here we synthesize protolith age constraints, and our structural, petrologic, and geochronologic data, and propose a revised tectonic model for the CBU on Syros. First we present a pre-subduction configuration, then discuss a stepwise reconstruction capturing progressive subduction, underplating, and exhumation, leading to the three-part tectonic stack exposed on Syros today.

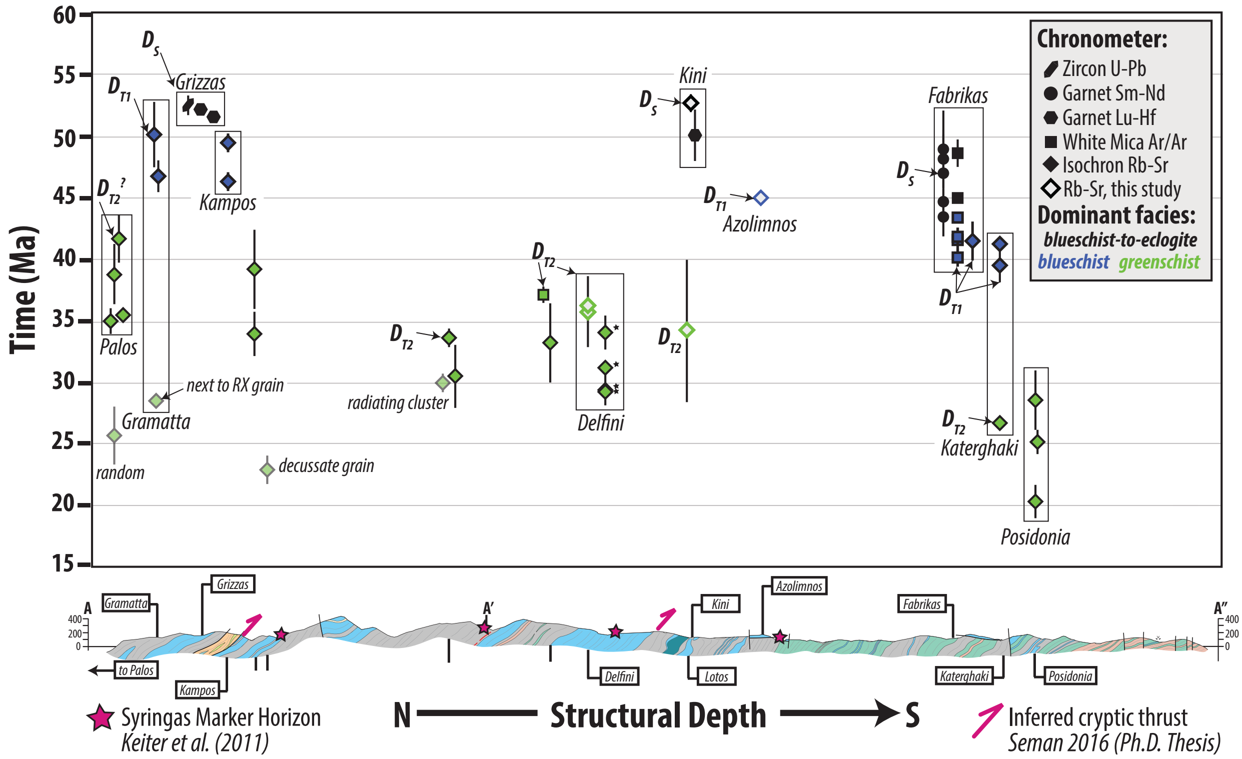

Figure 11: Metamorphic age vs. structural depth for the Syros nappe stack. The cross-section line A-A'-A" is shown in Figure 2. Only ages that were confidently linked to the deformation scheme outlined in this paper are included. Clusters of ages outlined in black boxes are derived from the same locality, and collapse onto a single point on the cross section. Delfini symbols marked with stars were reported as blueschist-facies fabrics by (Cliff et al., 2016); however, local preservation of glaucophane under greenschist facies conditions can be due to CO_2-bearing fluids.

7.1 Pre-subduction configuration

Figure 12 builds on previous work (e.g. Papanikolaou, 1987, 2013; Ring et al., 2010; Van Hinsbergen et al., 2020) and illustrates a schematic paleogeographic setting for the CBU on Syros and Southern Cyclades immediately prior to subduction at ∼60 Ma. Peri-Gondwanan Cycladic Basement, cross-cut by Carboniferous magmatism (∼315 on Syros, Tomaschek et al. (2008); 330-305 in Southern Cyclades, Flansburg et al. (2019)), was rifted in the Triassic (∼240 Ma, Keay (1998); Löwen et al. (2015)). Syn-rift bimodal volcanics and sediments intruded and blanketed the hyper-extended margin; these will become the diagnostic marker horizons referred to as banded tuffitic schists and bimodal meta-volcanics mapped by Keiter et al. (2011) (orange and dark grey in Fig. 12; cf. Fig. 2). Rifting was followed by passive margin sedimentation of psammites, debris flows, and carbonates from the Triassic (∼230) through the Cretaceous (∼75 Ma) (Löwen et al., 2015; Seman, 2016; Seman et al., 2017; Poulaki et al., 2019). Carbonates interbedded with clastic sediments may be the protolith for the Syringas Marker Horizon (Keiter et al., 2011). Cretaceous rifting (∼80 Ma, Tomaschek et al. (2003)) dissected the hyper-extended basement and passive margin sedimentary sequence, forming a small oceanic-affinity (backarc?) basin (Bonneau, 1984; Keiter et al., 2011; Fu et al., 2012; Cooperdock et al., 2018).

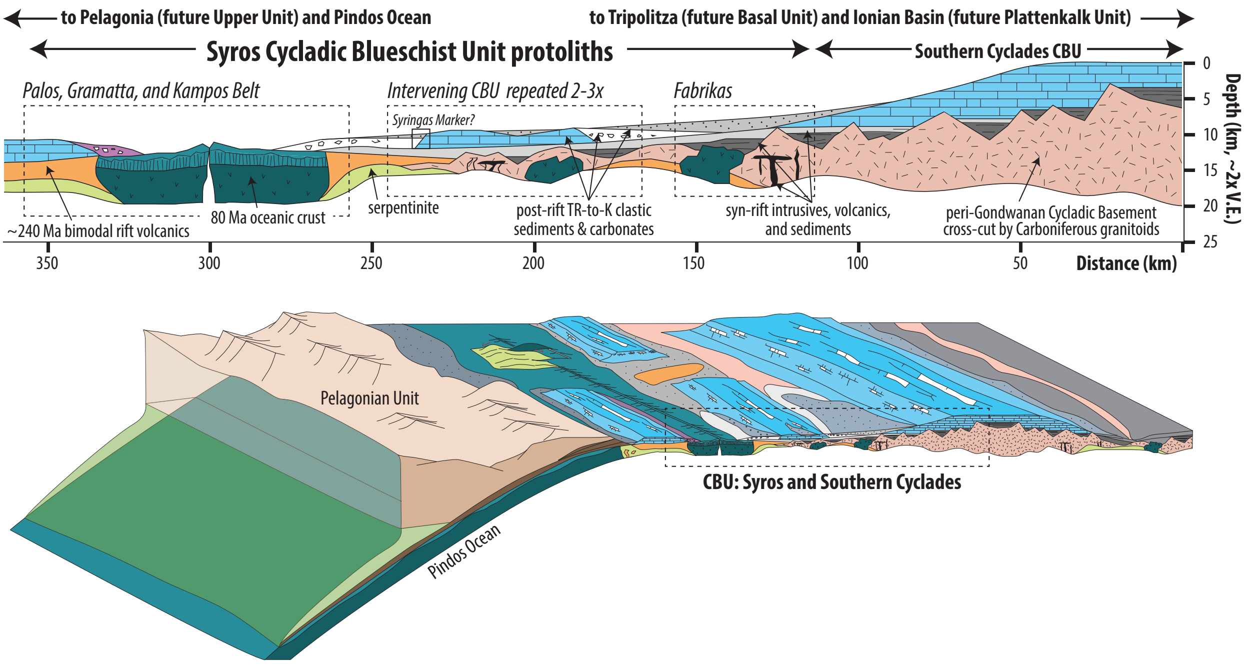

Figure 12: Schematic paleogeographic reconstruction of the CBU, with emphasis on lithologies exposed on Syros at ∼60 Ma. The zoomed-in cross section is modified from Seman (2016). Stepwise evolution of the CBU during subduction is shown in the next figure.

The most interpretive part of Figure 12 is the locations of mafic igneous rocks. These rocks could reflect off-axis, shallow intrusions related to Cretaceous rifting, or older mafic igneous rocks related to Triassic rifting; protolith ages have not been determined for Kini, Vaporia, Kalamisia, or Fabrikas mafic rocks. Regardless of their origin, the key point is that protoliths for mafic blueschists and eclogites were distributed throughout the CBU before subduction, rather than only coming from the small ocean basin in the north.

This paleogeographic interpretation allows us to split the CBU on Syros into three sub-domains characterized by distinct, but related, protolith assemblages (dashed boxes in Fig. 12). These sub-domains are the precursors to each of three main tectonic slices that comprise the structural pile on Syros today.

7.2 Peak subduction of the Palos-Gramatta-Kampos nappe (∼53 Ma)

The Palos-Gramatta-Kampos nappe (northern nappe) comprises Cretaceous oceanic lithosphere intruded into Triassic bimodal rift volcanics and Triassic-to-Cretaceous sediments (Fig. 12). Garnet Lu-Hf and new Rb-Sr isochrons sugguest that Kini was originally subducted as part of the northern nappe (Fig. 11), and was down-dropped by late-stage, high-angle normal faults to its present position (cf. Ridley, 1984; Keiter et al., 2011).

Prograde-to-peak subduction was characterized by extremely high asymmetric shear strain and at least two stages of foliation development under blueschist-to-eclogite-facies conditions (D_R and D_S; Fig. 13A). Yet, subduction-related strain was very heterogeneous. This is evidenced by rheologically strong meta-gabbros at Grizzas and Kini that preserve primary igneous features (Kotowski & Behr, 2019). Furthermore, early prograde SW-plunging fold axes and mineral lineations are preserved at Grizzas, Kini, and locally along Kampos Belt. Girdled glaucophane lineations (e.g. Kini, Kampos) record continuous kinematic rotation

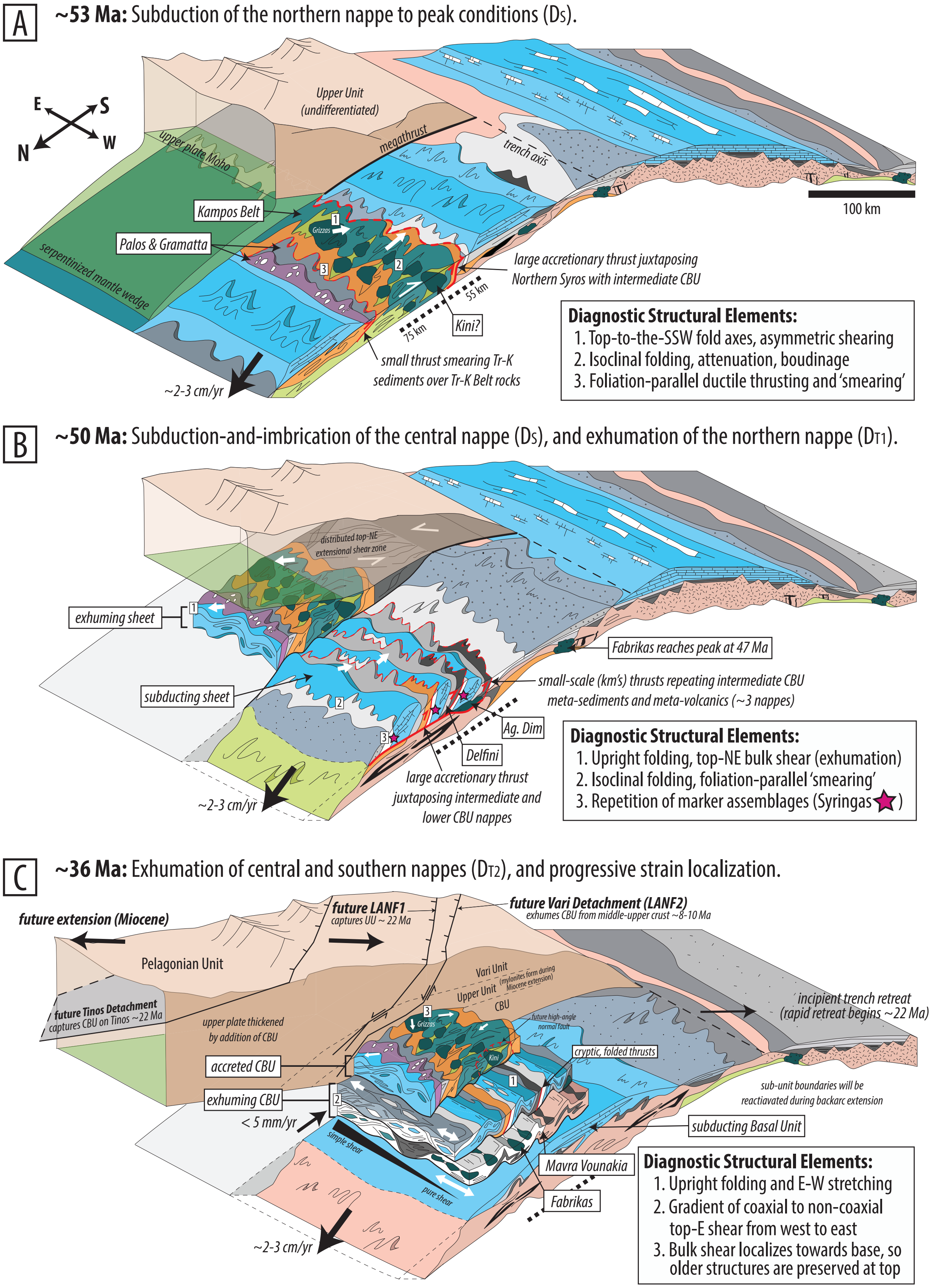

Figure 13: Caption on next page.

Figure 13: (Figure on previous page.) Block diagrams illustrating the structural evolution and timing of subduction and exhumation recorded by the three tectonic slices in the Syros nappe stack. Compare stepwise subduction of sub-units to the paleogeography in Figure 12. Horizontal scaling is equivalent to subduction rates of ∼2-3 cm/yr and diagrams are roughly 2x vertically exaggerated. The thickness of the interface is exaggerated for clarity.

from SW to N-S during subduction. Top-to-the-SW and top-to-the-S asymmetric thrusting are diagnostic of subduction kinematics (Blake Jr et al., 1981; Ridley, 1984; Keiter et al., 2004; Philippon et al., 2011; Laurent et al., 2016), indicated by SW-verging thrusts on mainland Greece (Jacobshagen, 1986). Furthermore, the preservation of a primary, young-on-old depositional relationship between Gramatta and Kampos indicates that the contact between the two has not been substantially disturbed during subduction and exhumation. However, some small-offset ductile thrusting likely 'smeared' the Palos-Gramatta meta-sedimentary rocks along the top of Kampos Belt volcanics (e.g. small thrust in Fig. 13A).

The northern nappe was underplated after D_S development and before D_T exhumation, removing it from the active subduction interface. DZ U-Pb data suggests that a large thrust separates the northern nappe from the central nappe beneath it (Seman, 2016) (Fig. 13A; structurally highest pink thrust in Fig. 11). This thrust placed Triassic and Cretaceous igneous rocks (Kampos) atop Cretaceous (Syringas) sediments and allowed the underplated nappe to exhume, while subduction of the intermediate nappe occurred beneath it.

7.3 Subduction-and-imbrication of the Syringas-Azolimnos nappe and blueschist facies exhumation of the northern nappe (∼50 Ma)

The Syringas-Vaporia-Azolimnos nappe (central nappe) occupies the central portion of the island and comprises interbedded Triassic-to-Cretaceous meta-sedimentary schists, meta-volcanic schists, and meta-carbonates (Fig. 12). The timing of peak D_S during subduction of the central nappe is unknown, but based on this tectonic model and the well-constrained ages of peak subduction in the northern and southern nappes, it likely reached peak conditions at ∼50 Ma (this is testable with garnet geochronology from Delfini, Agios Dimitrios, or Kalamisia). D_S in the central nappe is largely overprinted during subsequent exhumation-related deformation, but early fabrics are reminiscent of D_S in the northern nappe and similarly consist of isoclinal folds and strong cleavage development (e.g. textural relicts at Azolimnos). While D_S developed in the central nappe, D_{T1} exhumation-related blueschist facies fabrics formed at the same time in the northern nappe (Fig. 11, 13B).

MDAs calculated from DZ U-Pb of meta-sedimentary rocks in the central nappe reveal old-on-young stratigraphic inversions, which suggests imbrication occurred during subduction (Seman, 2016) (Fig. 13B). The locations of inferred thrusts are supported by the repeated Syringas Marker Horizon (pink stars in Fig. 11 and 13B) and Triassic bimodal meta-volcanic sequences (orange and dark grey in Figs. 2 and 13B). Thus, the central nappe is bounded by larger nappe-delimiting thrusts to its north and south, and also comprises smaller-scale thrusts accommodating internal imbrication of CBU meta-sedimentary rocks.

During subduction of the central nappe (D_S), D_{T1} deformation occurred in the northern nappe, and was characterized by upright folding, crenulation cleavage development, and NE-trending fold axes and mineral lineations. Continuous rotations of mineral lineations from the SW to the NE record this kinematic transition. We interpret the crenulation cleavage formed during D_{T1} to be a signature of the 'subduction-to-exhumation transition,' when rocks 'turn the corner' in the subduction channel, based on the observation that crenulation lineations are decorated by high-pressure phases with compositions similar to peak D_S blueschist-to-eclogite facies conditions (Kini, Figs. 6E). D_{T1} and subsequent strain localized in weaker CBU meta-sediments during exhumation (e.g. Palos, Gramatta), whereas prograde subduction-related fabrics are locally preserved in rheologically strong meta-gabbros at Grizzas and Kini.

The structural base of the central nappe is difficult to pinpoint. However, it is somewhere below Azolimnos and must be above the Fabrikas tectonostratigraphic horizon, which comprises the third and lowermost nappe. The presence of a nappe-bounding thrust is also consistent with progressive southward facies changes in the rock types, as carbonate horizons thin substantially, and gneissic material crops out at the island's southern tip. This ductile nappe-bounding structure accommodated underplating of the central nappe ∼50 Ma, while the southern nappe was subducting.

7.4 Peak subduction of the Fabrikas nappe and blueschist facies exhumation of the central nappe (∼47-45 Ma)

The Fabrikas nappe (southern nappe) comprises Triassic meta-sedimentary schists, meta-volcanic schists, and thinner meta-carbonate horizons compared to the central nappe (cf. Keiter et al., 2011); this meta-sedimentary sequence was spatially associated with mafic igneous rocks with unknown crystallization ages (Fig. 12). Peak subduction of the Fabrikas nappe is well-constrained at ∼47-45 Ma by garnet Sm-Nd crystallization ages (Kendall, 2016) and Ar/Ar of white micas in eclogites (Laurent et al., 2017) (Fig. 11) and is distinctly younger than peak subduction at ∼53 Ma of the northern nappe

Between ∼47-45 Ma, mafic blueschists and eclogites and surrounding meta-sedimentary schists in the central nappe developed identical D_{T1-2} structures (e.g. Vaporia and overlying meta-sedimentary rocks, and Kalamisia and Azolimnos, Fig. 4). This indicates that during D_{T1-2}, mafic blueschists and eclogites and surrounding meta-sedimentary rocks were exhumed together, and in some places, strain was partitioned between them. Therefore, even if mafic blueschists and eclogites reached higher pressures on their prograde path, they must have been partially exhumed and juxtaposed with CBU meta-sediments by ∼45 Ma to explain concordant exhumation-related structures.

7.5 Exhumation of the Syros nappe-stack in the subduction channel under greenschist facies conditions (44-20 Ma)

Between ∼44-20 Ma, greenschist facies D_{T2} fabrics continuously developed throughout the accreted CBU stack, younging systematically with structural depth, as each underplated nappe was exhumed in series from north to south. Exhumation imparted penetrative deformation that progressively transposed older fabrics under blueschist facies (D_{T1}) and eventually greenschist facies (D_{T2}) conditions. Exhumation-related D_{T1} and D_{T2} strain was dominantly coaxial and well-distributed. This is evident from symmetric strain shadows on garnets, ductile pinching of partially retrogressed eclogites at Agios Dimitrios, and outcrop-scale greenschist facies folds with sub-horizontal E-W trending hinge lines with hinge-parallel symmetric boudinage of competent blueschist and epidote-rich lenses (e.g. Delfini and Lotos; Figs. 5, C1).

The youngest dynamic D_{T2} greenschist facies fabrics associated with subduction channel exhumation are ∼25-20 Ma and are recorded in the southern nappe (Fig. 11). Meanwhile, in the northern and central nappes, greenschist facies metamorphism occurred locally, but was not associated with penetrative strain (e.g. random grains, radiating clusters, decussate textures; Cliff et al. (2016)). These observations indicate strain progressively localized towards the base of the stack through time. Patchy metamorphism in the northern and central nappes may reflect local fluid availability as the active interface migrated south.

7.6 Upper plate extension and core complex capture

Slab rollback began ∼22-18 Ma (Bröcker et al., 2004), leading to upper plate extension, core complex capture, and southward migration of the volcanic arc through the former forearc (e.g. the Tinos granite, 14-18 Ma, Altherr et al. (1982)). CBU rocks were exhumed in the footwall of the North and West Cycladic Detachment Systems and related smaller-scale structures during 'post-orogenic' exhumation (Jolivet et al., 2010; Soukis & Stockli, 2013). On Syros, this deformation is recorded by the Vari Detachment (Fig. 2).

Soukis and Stockli (2013) presented low-temperature zircon and apatite (U-Th)/He thermochronology, and concluded that the southern Syros CBU was juxtaposed with two structurally higher upper-plate units, the Upper Unit (intermediate structural level) and Vari Unit (structurally highest), along at least two semi-brittle detachment faults (Fig. 13C, labeled as future structures). While the Tinos Detachment exhumed CBU rocks between ∼22-19 on what would become neighboring Tinos Island, low-angle normal faults juxtaposed the Vari and Upper Units on Syros. Exhumation of the Vari and Upper Units at ∼13-15 Ma was roughly coeval with magmatism on Tinos but the Syros CBU exhumed later, ∼8-10 Ma, beneath the Vari Detachment (Soukis & Stockli, 2013). Final exhumation of the CBU on Syros occurred in multiple, temporally distinct, rapid episodes of unroofing. Exhumation beneath the Vari Detachment was rapid, but only accommodated the final ∼6-9 km of vertical exhumation (Ring et al., 2003).

8 Implications

The tectonic model described above has several similarities and differences compared to previous tectonic models. First, our results agree with Lister and Forster (2016) and Laurent et al. (2017) that Syros is composed of distinct tectonic slices that reached peak conditions at different times. Our study places quantitative constraints on the timing of subduction of each slice, and demonstrates that deformation occurred continuously throughout the Eocene and subduction- and exhumation-related fabrics developed contemporaneously at different structural levels. We argue that mafic blueschists and eclogites do *not* exclusively occupy the structurally highest tectonic slice, in contrast to Trotet et al. (2001a) and Laurent et al. (2016). Rather, protoliths for mafic blueschists and eclogites were present throughout the CBU before subduction and therefore appear to record primary relationships (cf. Keiter et al., 2011). This implies that the mafic blueschists and eclogites are not separated from surrounding schists and marbles by shear zones and/or detachments.

Our observations indicate that prograde textures are locally preserved in mafic blueschists and eclogites (cf. Keiter et al., 2004), but the majority of the Syros CBU has been overprinted during subduction channel exhumation (cf. Trotet et al., 2001b; Rosenbaum et al., 2002; Bond et al., 2007). Heterogeneous rock types that occupy a given nappe were subducted and exhumed together, and therefore experienced identical P-T paths (in contrast to Trotet et al. (2001b, 2001a)). Therefore, differences in strain, metamorphic mineral assemblages, and/or preserved kinematics between mafic blueschists and eclogites and meta-sedimentary rocks can be attributed to relative strengths, bulk composition, and fluid availability (and composition) during metamorphism.

Exhumation from peak depths was accommodated by well-distributed, ductile coaxial thinning throughout the bulk stack (cf. Rosenbaum et al., 2002; Bond et al., 2007) and resulted in penetrative Eocene-Oligocene blueschist and greenschist facies retrogression, unrelated to regional Miocene greenschist facies deformation. Non-coaxial deformation on the eastern and southeastern side of the island can be attributed to proximity to the Vari Detachment, which is thought to have operated as the extensional subduction channel roof (Laurent et al., 2016; Aravadinou & Xypolias, 2017). Compiled metamorphic geochronology and new Rb-Sr ages allow us to calculate exhumation rates of 1.5-5 mm/yr (= 1.5-5 km/Myr) for each underplated nappe. These rates are roughly an order of magnitude slower than subduction for the Hellenides, and are consistent with buoyancy-driven, channelized return flow in a distributed shear zone (Gerya et al., 2002; Warren et al., 2008; Burov et al., 2014). Furthermore, mm/yr exhumation rates are not consistent with fast rates (comparable to subduction rates) predicted for exhumation along deep-reaching, highly-localized detachments in an 'extrusion wedge' (e.g. Ring & Reischmann, 2002; Ring et al., 2020), nor with forced return flow and melange-like mixing in a low-viscosity wedge (Cloos, 1982; Gerya et al., 2002). Thus, between ~50 and ~25 Ma, return flow in the subduction channel accomplished *at least* 35 km, and potentially as much as 55 km of vertical exhumation from maximum depths to the greenschist facies middle crust (~4 kbar, ~15 km), accounting for ~75-80% of CBU exhumation.

On a regional scale, subduction, underplating, and syn-subduction exhumation were fundamental processes during construction of the greater Attic-Cycladic Complex (e.g. Trotet et al., 2001a; Jolivet et al., 2003; Ring & Layer, 2003; Lister & Forster, 2016; Laurent et al., 2017; Ring et al., 2020). CBU rocks on Sifnos have garnet crystallization ages of ~47-45 Ma (Dragovic et al., 2012, 2015), comparable to the base of the Syros stack. The Basal Unit reached peak conditions at ~33-27 Ma (Ring et al., 2007), contemporaneous with syn-subduction greenschist facies exhumation of the CBU on Syros (Fig. 11). The structurally deeper Phyllite-Quartzite Nappe and Plattenkalk unit exposed on Crete experienced HP/LT metamorphism between ~20-24 Ma (Seidel et al., 1982; Thomson et al., 1999), which also overlaps with latest stages of greenschist facies exhumation on Syros (Fig. 11). Extension and core complex capture that initiated during trench rollback reworked the ACC to its present configuration, and locally reactivated nappe-bounding thrusts as extensional structures (e.g. Vari Detachment on Syros).

9 Conclusions

Structural analysis, metamorphic petrology, and new and compiled geochronology demonstrate that exhumed HP/LT rocks on Syros Island (Cyclades, Greece) record progressive subduction, underplating, and return flow of three separate tectonic slices. Each nappe records a similar structural and metamorphic history, despite subducting at different times. Prograde subduction and underplating of each tectonic slice was characterized by asymmetric top-to-the-SSW and top-to-the-S shear strain, and was reached at ~53 Ma (northern nappe), ~50 Ma? (central nappe) and ~47 Ma (southern nappe). Prograde deformation and metamorphism is locally preserved in the northern and central nappes, but the majority of the island's meta-sedimentary lithologies were retrogressed during syn-orogenic blueschist-to-greenschist facies exhumation. The subduction-to-exhumation transition in each nappe is marked by systematic kinematic changes: dominant transport directions rotated from roughly N-S (syn-subduction), to NE (post-underplating, at the subduction-to-exhumation transition), to E-W (return flow) and the strain geometry switched from asymmetric to coaxial. Progressive subduction of structurally deeper nappes occurred contemporaneously with exhumation of structurally higher nappes throughout the Eocene and Oligocene, capturing syn-subduction exhumation in the Hellenic subduction zone. Subduction channel return flow proceeded at ~1.5-5 mm/yr (an order of magnitude slower than subduction), and accounted for ~80% of the vertical exhumation of the CBU. Continuous subduction, underplating, and syn-subduction exhumation appear to be fundamental processes during construction of the Attic-Cycladic Complex in the Central and Southern Cyclades.

Acknowledgments

This work was funded by an NSF Graduate Research Fellowship awarded to A.K., an NSF Career Grant (EAR-1555346) awarded to W.B., an NSF Grant (EAR-1725110) awarded to W.B., J.B., and D.S., a Jackson School Seed Grant awarded to J.B., W.B., and D.S., Jackson School Graduate Research Fellowships awarded to A.K. and M.C, and Ford

Foundation fellowship awarded to M.C. Many thanks to Staci Loewy and Aaron Satkoski (JSG, UT Austin) for help with Rb-Sr chemistry and isotope analyses, James Maner for assistance with the microprobe, and Emily Mixon for help with mineral separation. This project was part of A.K.'s Ph.D. dissertation and benefited from many conversations with Mark Cloos and Spencer Seman. The data that support the conclusions of this article are presented in the main text and in the supporting information. All data will be made publicly available in appropriate repositories, i.e. Pangaea (structural data), EarthChem (petrologic data), and Geochron (Rb-Sr data), before publication. The authors declare no conflicts of interest.

References

Agard, P., Plunder, A., Angiboust, S., Bonnet, G., & Ruh, J. (2018). The subduction plate interface: rock record and mechanical coupling (from long to short timescales). *Lithos*, *320*, 537–566.

Altherr, R., Kreuzer, H., Lenz, H., Wendt, I., Harre, W., & Dürr, S. (1994). Further evidence for a Late Cretaceous low-pressure/high-temperature terrane in the Cyclades, Greece. *Chemie der Erde*, *54*, 319–28.

Altherr, R., Kreuzer, H., Wendt, I., LENZ, H., & Wagner, G. (1982). A late oligocene/early miocene high temperature belt in the attic-cycladic crystalline complex (se pelagonian, greece). *Geologisches Jahrbuch. Reihe E, Geophysik*(23), 97–164.

Andriessen, P., Boelrijk, N., Hebeda, E. H., Priem, H., Verdurnen, E., & Verschure, R. H. (1979). Dating the events of metamorphism and granitic magmatism in the Alpine orogen of Naxos (Cyclades, Greece). *Contributions to Mineralogy and Petrology*, *69*(3), 215–225. doi: 10.1007/BF00372323

Angiboust, S., Agard, P., Glodny, J., Omrani, J., & Oncken, O. (2016). Zagros blueschists: Episodic underplating and long-lived cooling of a subduction zone. *Earth and Planetary Science Letters*, *443*, 48–58.

Aravadinou, E., & Xypolias, P. (2017). Evolution of a passive crustal-scale detachment (Syros, Aegean region): Insights from structural and petrofabric analyses in the hanging-wall. *Journal of Structural Geology*, *103*, 57–74.

Avigad, D., & Garfunkel, Z. (1989). Low-angle faults above and below a blueschist belt—Tinos Island, Cyclades, Greece. *Terra Nova*, *1*(2), 182–187.

Avigad, D., & Garfunkel, Z. (1991). Uplift and exhumation of high-pressure metamorphic terrains: the example of the Cycladic blueschist belt (Aegean Sea). *Tectonophysics*, *188*, 357–372.

Baldwin, S. L. (1996). Contrasting PTt histories for blueschists from the western Baja Terrane and the Aegean: Effects of synsubduction exhumation and backarc extension. *Washington DC American Geophysical Union Geophysical Monograph Series*, *96*, 135–141.

Ballevre, M., Pitra, P., & Bohn, M. (2003). Lawsonite growth in the epidote blueschists from the Ile de Groix (Armorican Massif, France): a potential geobarometer. *Journal of metamorphic Geology*, *21*(7), 723–735.

Baxter, E. F., & Caddick, M. J. (2013). Garnet growth as a proxy for progressive subduction zone dehydration. *Geology*, *41*(6), 643–646.

Behr, W. M., Kotowski, A. J., & Ashley, K. T. (2018). Dehydration-induced rheological heterogeneity and the deep tremor source in warm subduction zones. *Geology*, *46*(5), 475–478.

Behr, W. M., & Platt, J. P. (2012). Kinematic and thermal evolution during two-stage exhumation of a Mediterranean subduction complex. *Tectonics*, *31*(4). doi: 10.1029/2012TC003121

Blake Jr, M. C., Bonneau, M., Geyssant, J., Kienast, J., Lepvrier, C., H., & Papanikolaou, D. (1981). A geologic reconnaissance of the Cycladic blueschist belt, Greece. *Geological Society of America Bulletin*, *92*(5), 247–254.

Bond, C. E., Butler, R. W. H., & Dixon, J. E. (2007). Co-axial horizontal stretching within extending orogens: the exhumation of HP rocks on Syros (Cyclades) revisited. *Geological Society, London, Special Publications*, *272*(1), 203–222. Retrieved from `http://sp.lyellcollection.org/content/272/1/203.abstract` doi: 10.1144/GSL.SP.2007.272.01.12

Bonneau, M. (1984). Correlation of the Hellenide nappes in the south-east Aegean and their tectonic reconstruction. *Geological Society, London, Special Publications*, *17*(1), 517–527. Retrieved from `http://sp.lyellcollection.org/lookup/doi/10.1144/GSL.SP.1984.017.01.38` doi: 10.1144/GSL.SP.1984.017.01.38

Brichau, S., Ring, U., Carter, A., Monie, P., Bolhar, R., Stockli, D. F., & Brunel, M. (2007, jan). Extensional faulting on Tinos Island, Aegean Sea, Greece: How many detachments? *Tectonics*, *26*(4). Retrieved from papers3://publication/uuid/06DAB232-CF25-4D35-A7EB-F6A69A4DF869

Bröcker, M. (1990). Blueschist-to-greenschist transition in metabasites from Tinos Island, Cyclades, Greece: compositional control or fluid infiltration? *Lithos*, *25*, 25–39.

Bröcker, M., Baldwin, S., & Arkudas, R. (2013). The geological significance of 40Ar/39Ar and Rb-Sr white mica ages from Syros and Sifnos, Greece: A record of continuous (re)crystallization during exhumation? *Journal of Metamorphic Geology*, *31*(6), 629–646. doi: 10.1111/jmg.12037

Bröcker, M., Bieling, D., Hacker, B. R., & Gans, P. B. (2004, jan). High-Si phengite records the time of greenschist facies overprinting: implications for models suggesting mega-detachments in the Aegean Sea. *Journal of Metamorphic Geology*, *22*(5), 427–442. Retrieved from file:///Users/Behr-admin/Dropbox/Papers/Library.papers3/Articles/Br{\%}25C3{\%}25B6cker/2004/Br{\%}25C3{\%}25B6cker{_}JournalofMetamorphicGeology{_}2004.pdfpapers3://publication/uuid/810C9379-D791-4181-BD52-EEE52DC85F3D

Bröcker, M., & Enders, M. (1999, mar). U–Pb zircon geochronology of unusual eclogite-facies rocks from Syros and Tinos (Cyclades, Greece). *Geological Magazine*, *136*(02), 111–118. Retrieved from http://journals.cambridge.org.ezproxy.lib.utexas.edu/action/displayAbstract?aid=4743papers3://publication/uuid/ED377DC1-48F0-4823-835A-AD3673F219AF

Bröcker, M., & Enders, M. (2001, jun). Unusual bulk-rock compositions in eclogite-facies rocks from Syros and Tinos (Cyclades, Greece): implications for U–Pb zircon geochronology. *Chemical Geology*, *175*(3-4), 581–603. Retrieved from http://linkinghub.elsevier.com/retrieve/pii/S0009254100003697file:///Users/Behr-admin/Dropbox/Papers/Library.papers3/Articles/Br{\%}25C3{\%}25B6cker/2001/Br{\%}25C3{\%}25B6cker{_}ChemicalGeology{_}2001.pdfpapers3://publication/doi/10.1016/S0009-2541(00)00369-7

Bröcker, M., & Keasling, A. (2006, aug). Ionprobe U-Pb zircon ages from the high-pressure/low-temperature mélange of Syros, Greece: age diversity and the importance of pre-Eocene subduction. *Journal of Metamorphic Geology*, *24*(7), 615–631. Retrieved from http://doi.wiley.com/10.1111/j.1525-1314.2006.00658.xfile:///Users/Behr-admin/Dropbox/Papers/Library.papers3/Articles/Br{\%}25C3{\%}25B6cker/2006/Br{\%}25C3{\%}25B6cker{_}JournalofMetamorphicGeology{_}2006.pdfpapers3://publication/doi/10.1111/j.1525-1314.2006.00658.x

Bröcker, M., Kreuzer, H., Matthews, A., & Okrusch, M. (1993). 40Ar/39Ar and oxygen isotope studies of polymetamorphism from Tinos Island, Cycladic blueschist belt, Greece. *Journal of Metamorphic Geology*, *11*, 223–240.

Brown, E. (1977). The crossite content of ca-amphibole as a guide to pressure of metamorphism. *Journal of Petrology*, *18*(1), 53–72.

Brun, J.-P. P., & Faccenna, C. (2008, jan). Exhumation of high-pressure rocks driven by slab rollback. *Earth and Planetary Science Letters*, *272*, 1–7. Retrieved from http://linkinghub.elsevier.com/retrieve/pii/S0012821X08001416papers3://publication/uuid/E8FE17E1-C60B-4AC9-8C9F-4435EA549A1D

Bulle, F., Bröcker, M., Gärtner, C., & Keasling, A. (2010). Geochemistry and geochronology of HP mélanges from Tinos and Andros, Cycladic blueschist belt, Greece. *Lithos*, *117*(1-4), 61–81.

Burov, E., Francois, T., Yamato, P., & Wolf, S. (2014). Mechanisms of continental subduction and exhumation of HP and UHP rocks. *Gondwana Research*, *25*(2), 464–493.

Calvert, A. J., Preston, L. A., & Farahbod, A. M. (2011). Sedimentary underplating at the cascadia mantle-wedge corner revealed by seismic imaging. *Nature Geoscience*, *4*(8), 545–548.

Chemenda, A., Mattauer, M., Malavieille, J., & Bokun, A. (1995, jan). A mechanism for syn-collisional rock exhumation and associated normal faulting: Results from physical modelling. *Earth and Planetary Science Letters*, *132*, 225–232. Retrieved from http://linkinghub.elsevier.com/retrieve/pii/0012821X9500042Bpapers3://

publication/uuid/24846994-FAB6-4147-8883-2A2B9B1D53B5

Cisneros, M., Barnes, J., Behr, W. M., Kotowski, A. J., Stockli, D., & Soukis, K. (submitted). Insights from elastic thermobarometry into exhumation of high-pressure metamorphic rocks from syros, greece. *Solid Earth*.

Cliff, R. A., Bond, C. E., Butler, R. W. H., & Dixon, J. E. (2016, dec). Geochronological challenges posed by continuously developing tectonometamorphic systems; insights from Rb–Sr mica ages from the Cycladic Blueschist Belt, Syros (Greece). *J. Metamorph. Geol.*, doi:10.1111/jmg.12228. Retrieved from http://doi.wiley.com/10.1111/jmg.12228 doi: 10.1111/jmg.12228

Cliff, R. A., & Meffan-Main, S. (2003, jan). Evidence from Rb-Sr microsampling geochronology for the timing of Alpine deformation in the Sonnblick Dome, SE Tauern Window, Austria. *Geochronology: Linking the Isotopic Record with Petrology and Textures*, 159. Retrieved from papers3://publication/uuid/08ECF850-E95C-4774-B506-7043EE2BE72A

Cloos, M. (1982, jan). Flow melanges: Numerical modeling and geologic constraints on their origin in the Franciscan subduction complex, California. *GSA Bulletin*, *93*(4), 330. Retrieved from http://bulletin.geoscienceworld.org/cgi/content/abstract/93/4/330papers3://publication/uuid/388347B7-1AC8-4B74-B3B6-DC5C0E39C06A

Cloos, M. (1986). Blueschists in the Franciscan Complex of California: Petrotectonic constraints on uplift mechanisms. In *Blueschists and eclogites* (Vol. 164, pp. 77–93). Geological Society of America Memoir.

Cooperdock, E. H., Raia, N. H., Barnes, J. D., Stockli, D. F., & Schwarzenbach, E. M. (2018). Tectonic origin of serpentinites on Syros, Greece: Geochemical signatures of abyssal origin preserved in a HP/LT subduction complex. *Lithos*, *296*, 352–364.

Dixon, J. E. (1976). Glaucophane schists of Syros, Greece. *Bulletin de la Société géologique de France*, *7*(2), 280.

Dixon, J. E., & Ridley, J. (1987). Syros. In *Chemical transport in metasomatic processes* (Vol. 218, pp. 489–501). Reidel Publishing Company Dordrecht.

Dragovic, B., Baxter, E. F., & Caddick, M. J. (2015). Pulsed dehydration and garnet growth during subduction revealed by zoned garnet geochronology and thermodynamic modeling, Sifnos, Greece. *Earth and Planetary Science Letters*, *413*, 111–122.

Dragovic, B., Samanta, L. M., Baxter, E. F., & Selverstone, J. (2012). Using garnet to constrain the duration and rate of water-releasing metamorphic reactions during subduction: An example from Sifnos, Greece. *Chemical Geology*, *314*, 9–22.

Dürr, S., Altherr, R., Keller, J., Okrusch, M., & Seidel, E. (1978). The median Aegean crystalline belt: stratigraphy, structure, metamorphism, magmatism. *Alps, Apennines, Hellenides*, *38*, 455–476.

Ernst, W., & Liu, J. (1998). Experimental phase-equilibrium study of Al-and Ti-contents of calcic amphibole in MORB—a semiquantitative thermobarometer. *American mineralogist*, *83*(9-10), 952–969.

Evans, B. W. (1990). Phase relations of epidote-blueschists. *Lithos*, *25*(1-3), 3–23. doi: 10.1016/0024-4937(90)90003-J

Fagereng, Å., Savage, H., Morgan, J., Wang, M., Meneghini, F., Barnes, P., ... others (2019). Mixed deformation styles observed on a shallow subduction thrust, hikurangi margin, new zealand. *Geology*, *47*(9), 872–876.

Flansburg, M. E., Stockli, D. F., Poulaki, E. M., & Soukis, K. (2019). Tectono-magmatic and stratigraphic evolution of the Cycladic Basement, Ios Island, Greece. *Tectonics*.

Forster, M., & Lister, G. (2005). Several distinct tectono-metamorphic slices in the Cycladic eclogite–blueschist belt, Greece. *Contributions to Mineralogy and Petrology*, *150*(5), 523–545.

Forster, M., & Lister, G. (2008). Tectonic sequence diagrams and the structural evolution of schists and gneisses in multiply deformed terranes. *Journal of the Geological Society*, *165*(5), 923–939.

Freeman, S., Inger, S., Butler, R., & Cliff, R. A. (1997, jan). Dating deformation using Rb-Sr in white mica: Greenschist facies deformation ages .... *Tectonics*. Retrieved

from http://europa.agu.org/?uri=/journals/tc/96TC02477.xml{\&}view=articlepapers3://publication/uuid/E7B4274F-FDB0-40E7-8266-BBD52B38F230
Fu, B., Bröcker, M., Ireland, T., Holden, P., & Kinsley, L. P. (2015). Zircon U–Pb, O, and Hf isotopic constraints on Mesozoic magmatism in the Cyclades, Aegean Sea, Greece. *International Journal of Earth Sciences*, *104*(1), 75–87.
Fu, B., Paul, B., Cliff, J., Bröcker, M., & Bulle, F. (2012). O-Hf isotope constraints on the origin of zircon in high-pressure melange blocks and associated matrix rocks from Tinos and Syros, Greece. *European Journal of Mineralogy*, *24*(2), 277–287.
Gautier, P., Brun, J.-P., & Jolivet, L. (1993). Structure and kinematics of upper cenozoic extensional detachment on naxos and paros (cyclades islands, greece). *Tectonics*, *12*(5), 1180–1194.
Gerya, T. V., & Stöckhert, B. (2002, jan). Exhumation rates of high pressure metamorphic rocks in subduction channels: the effect of rheology. *Geophysical Research Letters*, *29*(8), 1261. Retrieved from papers3://publication/uuid/B673D8A0-155B-43D0-B5CF-7026FE19896B
Gerya, T. V., Stöckhert, B., & Perchuk, A. L. (2002, jan). Exhumation of high-pressure metamorphic rocks in a subduction channel: A numerical simulation. *Tectonics*, *21*(6), doi:10.1029/2002TC001406. Retrieved from http://www.agu.org/pubs/crossref/2002/2002TC001406.shtmlpapers3://publication/doi/10.1029/2002TC001406
Glodny, J., Austrheim, H., Molina, J. F., Rusin, A. I., & Seward, D. (2003). Rb/sr record of fluid-rock interaction in eclogites: The marun-keu complex, polar urals, russia. *Geochimica et Cosmochimica Acta*, *67*(22), 4353–4371.
Glodny, J., Kühn, A., & Austrheim, H. (2008, jan). Diffusion versus recrystallization processes in Rb–Sr geochronology: Isotopic relics in . . . . *Geochimica et Cosmochimica Acta*. Retrieved from http://linkinghub.elsevier.com/retrieve/pii/S0016703707006345papers3://publication/uuid/9FE00F83-E636-43B0-9933-35B5FCBFE721
Glodny, J., Ring, U., Kühn, A., Gleissner, P., & Franz, G. (2005, may). Crystallization and very rapid exhumation of the youngest Alpine eclogites (Tauern Window, Eastern Alps) from Rb/Sr mineral assemblage analysis. *Contributions to Mineralogy and Petrology*, *149*(6), 699–712. Retrieved from http://www.springerlink.com/index/U5PW505180300421.pdfpapers3://publication/doi/10.1007/s00410-005-0676-5
Grasemann, B., Schneider, D. A., Stockli, D. F., Iglseder, C., Stöckli, D. F., & Iglseder, C. (2012, jan). Miocene bivergent crustal extension in the Aegean: Evidence from the western Cyclades (Greece). *Lithosphere*, *4*(1), 23–39. Retrieved from http://lithosphere.gsapubs.org/cgi/doi/10.1130/L164.1papers3://publication/doi/10.1130/L164.1
Halama, R., Glodny, J., Konrad-Schmolke, M., & Sudo, M. (2018). Rb-sr and in situ 40ar/39ar dating of exhumation-related shearing and fluid-induced recrystallization in the sesia zone (western alps, italy). *Geosphere*, *14*(4), 1425–1450.
Hawthorne, F. C., Oberti, R., Harlow, G. E., Maresch, W. V., Martin, R. F., Schumacher, J. C., & Welch, M. D. (2012). Nomenclature of the amphibole supergroup. *American Mineralogist*, *97*(11-12), 2031–2048.
Hecht, J. (1985). Geological map of Greece 1: 50 000, Syros island. *Institute of Geology and Mineral Exploration, Athens*.
Inger, S., & Cliff, R. (1994). Timing of metamorphism in the tauern window, eastern alps: Rb-sr ages and fabric formation. *Journal of metamorphic Geology*, *12*(5), 695–707.
Jacobshagen, V. (1986). Geologie von Griechenland: Gebrüder Borntraeger. *Berlin-Stuttgart, 363pp*.
Jolivet, L., & Brun, J. P. (2010). Cenozoic geodynamic evolution of the Aegean. *International Journal of Earth Sciences*, *99*(1), 109–138. doi: 10.1007/s00531-008-0366-4
Jolivet, L., Faccenna, C., Goffé, B., Burov, E. B., & Agard, P. (2003, jan). Subduction tectonics and exhumation of high-pressure metamorphic rocks in the Mediterranean orogens. *American Journal of Science*, *303*(5),

353–409. Retrieved from http://ajsonline.org/cgi/content/abstract/303/5/353papers3://publication/uuid/313C27F4-1B1D-49D2-A7A3-953D704E5793

Jolivet, L., Faccenna, C., Huet, B., Labrousse, L., Le Pourhiet, L., Lacombe, O., ... Driussi, O. (2013). Aegean tectonics: Strain localisation, slab tearing and trench retreat. *Tectonophysics*, *597-598*, 1–33. doi: 10.1016/j.tecto.2012.06.011

Jolivet, L., Trotet, F., Monie, P., Vidal, O., Goffé, B., Labrousse, L., ... Ghorbal, B. (2010, jan). Along-strike variations of PT conditions in accretionary wedges and syn-orogenic extension, the HP-LT Phyllite-Quartzite Nappe in Crete and the Peloponnese. *Tectonophysics*, *480*(1-4), 133–148. Retrieved from papers3://publication/uuid/05D78E1D-3C49-4CA6-98C3-97A752D40E1F

Keay, S. (1998). *The geological evolution of the Cyclades, Greece: constraints from SHRIMP U-Pb geochronology* (Unpublished doctoral dissertation).

Keay, S., & Lister, G. (2002). African provenance for the metasediments and metaigneous rocks of the Cyclades, Aegean Sea, Greece. *Geology*, *30*(3), 235–238.

Keiter, M., Ballhaus, C., & Tomaschek, F. (2011). A new geological map of the Island of Syros (Aegean Sea, Greece): Implications for lithostratigraphy and structural history of the Cycladic Blueschist Unit. *Geol. Soc. Am. Spec. Pap.*, *481*, 1–43.

Keiter, M., Piepjohn, K., Ballhaus, C., Lagos, M., & Bode, M. (2004, aug). Structural development of high-pressure metamorphic rocks on Syros island (Cyclades, Greece). *Journal of Structural Geology*, *26*(8), 1433–1445. Retrieved from http://linkinghub.elsevier.com/retrieve/pii/S0191814103002062papers3://publication/doi/10.1016/j.jsg.2003.11.027http://www.sciencedirect.com/science/article/pii/S0191814103002062papers3://publication/uuid/9F769F57-8390-43F0-8D62-C74BBB0F90B4

Kendall, J. (2016). *Sm/nd garnet geochronology and pressure-temperature paths of eclogites from syros, greece: Implications for subduction zone processes and water loss from the subducting slab* (Unpublished doctoral dissertation). Boston College.

Kimura, H., Takeda, T., Obara, K., & Kasahara, K. (2010). Seismic evidence for active underplating below the megathrust earthquake zone in japan. *Science*, *329*(5988), 210–212.

Kirchner, K. L., Behr, W. M., Loewy, S., & Stockli, D. F. (2016). Early Miocene subduction in the western Mediterranean, constraints from Rb-Sr multi-mineral isochron geochronology. *Geochem. Geophys. Geosyst.*, *17*(5), doi:10.1002/2015GC006208. doi: 10.1002/2015GC006208

Kleine, B. I., Skelton, A. D., Huet, B., & Pitcairn egu045., I. K. . (2014). Preservation of Blueschist-facies Minerals along a Shear Zone by Coupled Metasomatism and Fast-flowing CO2-bearing Fluids. *Journal of Petrology*, *55*, 1905–1939.

Kotowski, A. J., & Behr, W. M. (2019). Length scales and types of heterogeneities along the deep subduction interface: Insights from exhumed rocks on Syros Island, Greece. *Geosphere*, *15*(4), 1038–1065.

Kullerud, L. (1991). On the calculation of isochrons. *Chemical Geology: Isotope Geoscience section*, *87*(2), 115–124.

Lagos, M., Scherer, E. E., Tomaschek, F., Münker, C., Keiter, M., Berndt, J., & Ballhaus, C. (2007, jan). High precision Lu–Hf geochronology of Eocene eclogite-facies rocks from Syros, Cyclades, Greece. *Chemical Geology*, *243*(1), 16–35. Retrieved from http://www.sciencedirect.com/science/article/pii/S0009254107001751papers3://publication/uuid/77497147-A4FC-4D87-B574-681BE0904700

Laird, J., & Albee, A. L. (1981). Pressure, temperature, and time indicators in mafic schist; their application to reconstructing the polymetamorphic history of Vermont. *American Journal of Science*, *281*(2), 127–175.

Lanari, P., & Duesterhoeft, E. (2018). Modeling metamorphic rocks using equilibrium thermodynamics and internally consistent databases: past achievements, problems and perspectives. *Journal of petrology*, *60*(1), 19–56.

Lanari, P., & Engi, M. (2017). Local bulk composition effects on metamorphic mineral assemblages. *Reviews in Mineralogy and Geochemistry*, *83*(1), 55–102.

Lanari, P., Giuntoli, F., Loury, C., Burn, M., & Engi, M. (2017). An inverse modeling approach to obtain P–T conditions of metamorphic stages involving garnet growth and resorption. *European Journal of Mineralogy*, *29*(2), 181–199.

Laurent, V., Huet, B., Labrousse, L., Jolivet, L., Monie, P., & Augier, R. (2017). Extraneous argon in high-pressure metamorphic rocks: Distribution, origin and transport in the Cycladic Blueschist Unit (Greece). *Lithos*, *272*, 315–335.

Laurent, V., Jolivet, L., Roche, V., Augier, R., Scaillet, S., & Cardello, G. L. (2016). Strain localization in a fossilized subduction channel: Insights from the Cycladic Blueschist Unit (Syros, Greece). *Tectonophysics*, *672*(150-169). doi: 10.1016/j.tecto.2016.01.036

Laurent, V., Lanari, P., Naïr, I., Augier, R., Lahfid, A., & Jolivet, L. (2018). Exhumation of eclogite and blueschist (Cyclades, Greece): Pressure–Temperature evolution determined by thermobarometry and garnet equilibrium modelling. *Journal of Metamorphic Geology*.

Leake, B. E., Wooley, A. R., Arps, C. E., Birch, W. D., Gilbert, M. C., Grice, J. D., ... others (1997). Nomenclature of amphiboles; report of the subcommittee on amphiboles of the international mineralogical association commission on new minerals and mineral names. *European Journal of Mineralogy*, *9*(3), 623–651.

Liou, J. (1971). P—T stabilities of laumontite, wairakite, lawsonite, and related minerals in the system CaAl2Si2O8-SiO2-H2O. *Journal of Petrology*, *12*(2), 379–411.

Lister, G., & Forster, M. (2016). White mica 40Ar/39Ar age spectra and the timing of multiple episodes of high-P metamorphic mineral growth in the Cycladic eclogite–blueschist belt, Syros, Aegean Sea, Greece. *Journal of Metamorphic Geology*, *34*(5), 401–421.

Liu, F., Gerdes, A., Liou, J., Xue, H., & Liang, F. (2006). Shrimp u-pb zircon dating from sulu-dabie dolomitic marble, eastern china: constraints on prograde, ultrahigh-pressure and retrograde metamorphic ages. *Journal of metamorphic Geology*, *24*(7), 569–589.

Löwen, K., Bröcker, M., & Berndt, J. (2015). Depositional ages of clastic metasediments from Samos and Syros, Greece: results of a detrital zircon study. *International Journal of Earth Sciences*, *104*(1), 205–220.

Maluski, H., Bonneau, M., & Kienast, J. R. (1987). Dating the metamorphic events in the Cycladic area; 39Ar/40 Ar data from metamorphic rocks of the Island of Syros (Greece). *Bull. Société Géologique Fr.*, *3*, 833–842.

Maruyama, S., Suzuki, K., & Liou, J. (1983). Greenschist–amphibolite transition equilibria at low pressures. *Journal of Petrology*, *24*(4), 583–604.

Massonne, H.-J., & Schreyer, W. (1987). Phengite geobarometry based on the limiting assemblage with K-feldspar, phlogopite, and quartz. *Contributions to Mineralogy and Petrology*, *96*(2), 212–224.

Moody, J. B., Meyer, D., & Jenkins, J. E. (1983). Experimental characterization of the greenschist/amphibolite boundary in mafic systems. *American Journal of Science*, *283*(1), 48–92.

Müller, W., Dallmeyer, R. D., Neubauer, F., & Thöni, M. (1999). Deformation-induced resetting of rb/sr and 40ar/39ar mineral systems in a low-grade, polymetamorphic terrane (eastern alps, austria). *Journal of the Geological Society*, *156*(2), 261–278.

Okrusch, M., & Bröcker, M. (1990, jan). Eclogites associated with high-grade blueschists in the Cyclades archipelago, Greece; a review. *European Journal of Mineralogy*, *2*(4), 451–478. Retrieved from `http://eurjmin.geoscienceworld.org/content/2/4/451.shortpapers3://publication/uuid/50C6E894-B8CD-4559-9D35-4FFCBA81AA18`

Okrusch, M., Seidel, E., & Davis, E. N. (1978). The assemblage jadeite-quartz in the glaucophane rocks of Sifnos (Cyclades Archipelago, Greece). *N Jb Mineral Abh*, *132*, 284–308.

Otsuki, M., & Banno, S. (1990). Prograde and retrograde metamorphism of hematitebearing basic schists in the sanbagawa belt in central shikoku. *Journal of Metamorphic Geology*, *8*(4), 425–439.

Papanikolaou, D. (1987). Tectonic evolution of the Cycladic blueschist belt (Aegean Sea, Greece). In *Chemical transport in metasomatic processes* (Vol. 218, pp. 429–450).

Papanikolaou, D. (2013, jun). Tectonostratigraphic models of the Alpine terranes and subduction history of the Hellenides. *Tectonophysics*, *595-596*, 1–24. Retrieved from `http://linkinghub.elsevier.com/retrieve/pii/S0040195112004854papers3://publication/doi/10.1016/j.tecto.2012.08.008`

Park, J.-O., Tsuru, T., Takahashi, N., Hori, T., Kodaira, S., Nakanishi, A., ... Kaneda, Y. (2002). A deep strong reflector in the nankai accretionary wedge from multichannel seismic data: Implications for underplating and interseismic shear stress release. *Journal of Geophysical Research: Solid Earth*, *107*(B4), ESE–3.

Pe-Piper, G., Piper, D. J., & Matarangas, D. (2002). Regional implications of geochemistry and style of emplacement of Miocene I-type diorite and granite, Delos, Cyclades, Greece. *Lithos*, *60*(1-2), 47–66.

Philippon, M., Brun, J. P., & Gueydan, F. (2011, jan). Tectonics of the Syros blueschists (Cyclades, Greece): From subduction to Aegean extension. *Tectonics*, *30*, TC4001, doi:10.1029/2010TC002810.

Philippon, M., Brun, J. P., & Gueydan, F. (2012, jan). Deciphering subduction from exhumation in the segmented Cycladic Blueschist Unit (Central Aegean, Greece). *Tectonophysics*.

Platt, J. P. (1993, jan). Exhumation of high-pressure rocks: a review of concepts and processes. *Terra Nova*, *5*, 119–133. Retrieved from `http://acad.coloradocollege.edu/dept/gy/ises/docs/Platt{\_}1993{\_}Exhumation.pdfpapers3://publication/uuid/5EBBB563-EB8E-4E5A-8BA8-A49488B06448`

Platt, J. P., Soto, J. I., Whitehouse, M. J., Hurford, A. J., & Kelley, S. P. (1998, jan). Thermal evolution, rate of exhumation, and tectonic significance of .... *Tectonics*. Retrieved from `http://earth.usc.edu/{~}jplatt/pdfs/PlattetalTect1998.pdfpapers3://publication/uuid/9D98D93B-8C39-4333-9426-DDE259D4F338`

Platt, J. P., Xia, H., & Schmidt, W. L. (2018). Rheology and stress in subduction zones around the aseismic/seismic transition. *Progress in Earth and Planetary Science*, *5*, 1–12.

Poulaki, E. M., Stockli, D. F., Flansburg, M. E., & Soukis, K. (2019). Zircon u-pb chronostratigraphy and provenance of the cycladic blueschist unit and the nature of the contact with the cycladic basement on sikinos and ios islands, greece. *Tectonics*.

Powell, R., Hergt, J., & Woodhead, J. (2002). Improving isochron calculations with robust statistics and the bootstrap. *Chemical Geology*, *185*(3-4), 191–204.

Putlitz, B., Cosca, M. A., & Schumacher, J. C. (2005, jan). Prograde mica 40Ar/39Ar growth ages recorded in high pressure rocks (Syros, Cyclades, Greece). *Chemical Geology*, *214*(1-2), 79–98. Retrieved from `http://linkinghub.elsevier.com/retrieve/pii/S0009254104003547`

Raase, P. (1974). Al and Ti contents of hornblende, indicators of pressure and temperature of regional metamorphism. *Contributions to mineralogy and petrology*, *45*(3), 231–236.

Ridley, J. R. (1982). Arcuate lineation trends in a deep level, ductile thrust belt, syros, Greece. *Tectonophysics*, *88*(3-4), 347–360. doi: 10.1016/0040-1951(82)90246-3

Ridley, J. R. (1984, jan). The significance of deformation associated with blueschist facies metamorphism on the Aegean island of Syros. *Geological Society, London, Special Publications*, *17*(1), 545–550.

Ring, U., Glodny, J., Will, T., & Thomson, S. (2010, jan). The Hellenic subduction system: high-pressure metamorphism, exhumation, normal faulting, and large-scale extension. *Annual Review of Earth and Planetary Sciences*, *38*, 45–76. Retrieved from `http://www.annualreviews.org/doi/abs/10.1146/annurev.earth.050708.170910papers3://publication/doi/10.1146/annurev.earth.050708.170910`

Ring, U., & Layer, P. W. (2003). High-pressure metamorphism in the Aegean, eastern Mediterranean: Underplating and exhumation from the Late Cretaceous until the Miocene to Recent above the retreating Hellenic subduction zone. *Tectonics*, *22*(3).

Ring, U., Pantazides, H., Glodny, J., & Skelton, A. (2020). Forced return flow deep in the subduction channel, syros, greece. *Tectonics*, *39*(1), e2019TC005768.

Ring, U., & Reischmann, T. (2002). The weak and superfast Cretan detachment, Greece: exhumation at subduction rates in extruding wedges. *Journal of the Geological Society*, *159*, 225–228. doi: 10.1144/0016-764901-150

Ring, U., Thomson, S. N., & Bröcker, M. (2003). Fast extension but little exhumation: the Vari detachment in the Cyclades, Greece. *Geological Magazine*, *140*(3), 245–252.

Ring, U., Will, T., Glodny, J., Kumerics, C., Gessner, K., Thomson, S., & Drüppel, K. (2007, jan). Early exhumation of high-pressure rocks in extrusion wedges: Cycladic blueschist unit in the eastern Aegean, Greece, and Turkey. *Tectonics*, *26*, TC2001. Retrieved from `http://www.agu.org/pubs/crossref/2007.../2005TC001872.shtmlpapers3://publication/uuid/11FA1518-AD95-4182-9BE4-2B6413C8D45F`

Robertson, A. H. F. (2007). Overview of tectonic settings related to the rifting and opening of Mesozoic ocean basins in the Eastern Tethys: Oman, Himalayas and Eastern Mediterranean regions. *Geological Society, London, Special Publications*, *282*(1), 325–388.

Robinson, P. (1982). Phase relations of metamorphic amphiboles: Natural occurences and theory. *Rev. Mineral.*, *9*, 1–227.

Rogowitz, A., Huet, B., Schneider, D., & Grasemann, B. (2015). Influence of high strain rate deformation on 40ar/39ar mica ages from marble mylonites (syros, greece). *Lithosphere*, *7*(5), 535–540.

Rondenay, S., Abers, G. A., & van Keken, P. E. (2008, jan). Seismic imaging of subduction zone metamorphism. *Geology*, *36*(4), 274–275. Retrieved from `http://geology.gsapubs.org/cgi/doi/10.1130/G24112A.1papers3://publication/doi/10.1130/G24112A.1`

Rosenbaum, G., Avigad, D., & Sánchez-Gómez, M. (2002, jan). Coaxial flattening at deep levels of orogenic belts: evidence from blueschists and eclogites on Syros and Sifnos (Cyclades, Greece). *Journal of Structural Geology*, *24*, 1451–1462.

Schliestedt, M. (1986). Eclogite-blueschist relationships as evidenced by mineral equilibria in the high-pressure metabasic rocks of sifnos (Cycladic Islands), Greece. *Journal of Petrology*, *27*(6), 1437–1459. doi: 10.1093/petrology/27.6.1437

Schmidt, M. W. (1992). Amphibole composition in tonalite as a function of pressure: an experimental calibration of the Al-in-hornblende barometer. *Contributions to mineralogy and petrology*, *110*(2-3), 304–310.

Schneider, D. A., Grasemann, B., Lion, A., Soukis, K., & Draganits, E. (2018). Geodynamic significance of the Santorini Detachment System (Cyclades, Greece). *Terra Nova*.

Schumacher, J. C., J.B., B., Cheney, J. T., Tonnsen, R. R., Brady, J. B., Cheney, J. T., & Tonnsen, R. R. (2008, aug). Glaucophane-bearing Marbles on Syros, Greece. *J. Petrology*, *49*(9), 1667–1686. Retrieved from `http://www.petrology.oxfordjournals.org/cgi/doi/10.1093/petrology/egn042papers3://publication/doi/10.1093/petrology/egn042`

Seck, H. A., Koetz, J., Okrusch, M., Seidel, E., & Stosch, H.-G. (1996). Geochemistry of a meta-ophiolite suite: an association of metagabbros, eclogites and glaucophanites on the island of Syros, Greece. *European Journal of Mineralogy*, 607–624.

Seidel, E., Kreuzer, H., & Harre, W. (1982). A late oligocene/early miocene high pressure belt in the external hellenides. *Geologisches Jahrbuch. Reihe E, Geophysik*(23), 165–206.

Seman, S. (2016). *The tectonostratigraphy of the Cycladic Blueschist Unit and new garnet geo/thermochronology techniques* (Unpublished doctoral dissertation).

Seman, S., Stockli, D., & Soukis, K. (2017). The provenance and internal structure of the Cycladic Blueschist Unit revealed by detrital zircon geochronology, Western Cyclades, Greece. *Tectonics*, *36*(7), 1407–1429.

Skelton, A., Peillod, A., Glodny, J., Klonowska, I., Månbro, C., Lodin, K., & Ring, U. (2019). Preservation of high-P rocks coupled to rock composition and the absence of metamorphic fluids. *Journal of Metamorphic Geology*.

Soukis, K., & Stockli, D. F. (2013, jan). Structural and thermochronometric evidence for multi-stage exhumation of southern Syros, Cycladic islands, Greece. *Tectono-*

physics, *595-596*, 148–164. Retrieved from `http://www.sciencedirect.com/science/article/pii/S0040195112002806papers3://publication/uuid/E4EA6C10-9045-4A74-AF9D-0D016D22F6A8`

Thompson, R. (1974). Some high-pressure pyroxenes. *Mineralogical Magazine*, *39*(307), 768–787.

Thomson, S. N., Stöckhert, B., & Brix, M. R. (1999). Miocene high-pressure metamorphic rocks of crete, greece: rapid exhumation by buoyant escape. *Geological Society, London, Special Publications*, *154*(1), 87–107.

Tomaschek, F., Keiter, M., Kennedy, A. K., & Ballhaus, C. (2008). Pre-Alpine basement within the Northern Cycladic Blueschist Unit on Syros Island, Greece [Präalpines Grundgebirge in der Nördlichen Kykladischen Blauschiefereinheit auf der Insel Syros, Griechenland.]. *Zeitschrift der deutschen Gesellschaft für Geowissenschaften*, *159*(3), 521–531.

Tomaschek, F., Kennedy, A. K., Villa, I. M., Lagos, M., & Ballhaus, C. (2003). Zircons from Syros, Cyclades, Greece—recrystallization and mobilization of zircon during high-pressure metamorphism. *Journal of Petrology*, *44*(11), 1977–2002.

Trotet, F., Jolivet, L., & Vidal, O. (2001a). Tectono-metamorphic evolution of Syros and Sifnos islands (Cyclades, Greese). *Tectonophysics*, *338*(2), 179–206. doi: 10.1016/S0040-1951(01)00138-X

Trotet, F., Vidal, O., & Jolivet, L. (2001b). Exhumation of Syros and Sifnos metamorphic rocks (Cyclades, Greece). New constraints on the PT paths. *European Journal of Mineralogy*, *13*(5), 901–902.

Ukar, E., Cloos, M., & Vasconcelos, P. (2012). First 40ar-39ar ages from low-t mafic blueschist blocks in a franciscan mélange near san simeon: Implications for initiation of subduction. *The Journal of Geology*, *120*(5), 543–556.

Uunk, B., Brouwer, F., ter Voorde, M., & Wijbrans, J. (2018). Understanding phengite argon closure using single grain fusion age distributions in the Cycladic Blueschist Unit on Syros, Greece. *Earth and Planetary Science Letters*, *484*, 192–203.

van der Maar, P. A., & Jansen, J. B. H. (1983). The geology of the polymetamorphic complex of Ios, Cyclades, Greece and its significance for the Cycladic Massif. *Geologische Rundschau*, *72*(1), 283–299.

Van Hinsbergen, D. J., Torsvik, T. H., Schmid, S. M., Maţenco, L. C., Maffione, M., Vissers, R. L., ... Spakman, W. (2020). Orogenic architecture of the mediterranean region and kinematic reconstruction of its tectonic evolution since the triassic. *Gondwana Research*, *81*, 79–229.

Vermeesch, P. (2018). Isoplotr: A free and open toolbox for geochronology. *Geoscience Frontiers*, *9*(5), 1479–1493.

Villa, I. M., De Bièvre, P., Holden, N., & Renne, P. (2015). Iupac-iugs recommendation on the half life of 87rb. *Geochimica et Cosmochimica Acta*, *164*, 382–385.

Wakabayashi, J. (1990). Counterclockwise PTt paths from amphibolites, Franciscan Complex, California: Relics from the early stages of subduction zone metamorphism. *The Journal of Geology*, *98*(5), 657–680.

Warren, C. J., Beaumont, C., & Jamieson, R. A. (2008, apr). Formation and exhumation of ultra-high-pressure rocks during continental collision: Role of detachment in the subduction channel. *Geochem. Geophys. Geosyst*, *9*(4). Retrieved from `http://doi.wiley.com/10.1029/2007GC001839papers3://publication/doi/10.1029/2007GC001839`

Wendt, I., & Carl, C. (1991). The statistical distribution of the mean squared weighted deviation. *Chemical Geology: Isotope Geoscience Section*, *86*(4), 275–285.

Wijbrans, J. R., Schliestedt, M., & York, D. (1990). Single grain argon laser probe dating of phengites from the blueschist to greenschist transition on Sifnos (Cyclades, Greece). *Contributions to Mineralogy and Petrology*, *104*, 582–593.

Xia, H., & Platt, J. P. (2017). Structural and rheological evolution of the Laramide subduction channel in southern California. *Solid Earth*, *8*(2).

Yakymchuk, C., Clark, C., & White, R. W. (2017). Phase relations, reaction sequences and petrochronology. *Reviews in Mineralogy and Geochemistry*, *83*(1), 13–53.